

이화여자대학교 대학원
2019학년도
석사학위 청구논문

Muscle-based Real-time
Facial Animation using Shell Elements
and Force Decomposition

컴퓨터공학과

Jungmin Kim

2020

Muscle-based Real-time Facial Animation using Shell Elements and Force Decomposition

이 논문을 석사학위 논문으로 제출함

2019 년 12 월

이화여자대학교 대학원

컴퓨터공학과 Jungmin Kim

Jungmin Kim 의 석사학위 논문을 인준함

지도교수 김 영 준 _____

심사위원 박 현 석 _____

오 유 란 _____

김 영 준 _____

이화여자대학교 대학원

Table of Contents

Table of Contents	i
List of Figures	iii
List of Tables	v
Abstract	vi
I. Introduction	1
A. Motivation	1
B. Research Goal.....	2
C. Challenges	2
D. Main Contributions	3
II. Related Work	5
A. Muscle-based Modeling	5
B. Facial Animation	6
1. Kinematic Approach	6
2. Facial Rigging	8
3. Dynamic Approach with Anatomical Properties	9
III. Real-time Thin Shell Simulation using Modal Warping	12
A. Real-time Thin Shell Simulation	12
B. Modal Warping	14
IV. Muscle-based Face Model	16
A. Simplified Design of Anatomical Structure	16
B. 3D Modeling for Physics-based Facial System.....	18
V. Physics for Face Model	20
A. Muscle Deformation Control.....	20
B. Force Propagation through the Subcutaneous Layer to the Skin.....	23
VI. Force Decomposition for Combined Facial Deformation	26
VII. Experimental Results	28

A. Implementation Details	28
B. Mesh Generation	29
C. Simulation Results.....	30
1. Muscle Deformation.....	30
2. Skin Deformation.....	31
VIII. Conclusion.....	42
Bibliography	43
Appendix I	47
Appendix II.....	48
국문초록	49

List of Figures

Figure 1. Muscle-based animation for human bodies	5
Figure 2. Multi-scaled facial animation with marker-based motion capture [2]	6
Figure 3. Markerless tracking for real-time facial animation of the virtual avatar using Kinect [17].....	7
Figure 4. Facial rigging with FACS	8
Figure 5. Facial rigging considering muscle positions.	9
Figure 6. Lattice structure mimicking anatomical properties of the face	10
Figure 7. Physics-based facial simulation with an anatomically-designed system	11
Figure 8. The anatomical structure of the face.....	16
Figure 9. Simplified structure of a face model.....	17
Figure 10. Muscle mesh modeled and positioned with template skin and skull mesh	18
Figure 11. Tessellation of muscle mesh	19
Figure 12. Constrained and enforced muscle nodes	21
Figure 13. Mass-spring force direction according to muscle and skin attached to it	24
Figure 14. Decoupling and integrating the displacement field of skin mesh.....	27
Figure 15. Plug-in and the connections with input and output mesh.....	28
Figure 16. Skin, muscle, and skull mesh for face model	29
Figure 17. Muscle deformation by external tangential force with static constraint points	30
Figure 18. Facial muscle, corresponding ROI, and skin deformation due to the contraction of the right muscle and both the left and right muscles (left to right for each row).....	33
Figure 19. Insertion and ROI of corrugator supercilii	34
Figure 20. Skin deformation due to contraction (center to left) and relaxation (center to right) of corrugator supercilii from the neutral face (center).....	34
Figure 21. Static constraints of skin for gravity load.....	35

Figure 22. Gravity load for skin with decreasing element stiffnesses	35
Figure 23. Frame by frame animation for simultaneous deformation of multiple muscles causing combined skin deformation.....	37
Figure 24. Static constraints and corresponding displacement field of Fexts1 ..	38
Figure 25. Skin deformation caused by concurrent effects by Fexts1 and contraction of zygomaticus major	38
Figure 26. Transition between the lifted lip and pulled down lip from the t_0 to t_3 time interval about 80 FPS	40
Figure 27. Facial animation with user-specific mesh	41
Figure 28. Edge indices information.....	47

List of Tables

Table 1. Number# of nodes, elements, and edges for simulation meshes.....	29
Table 2. Simulation performance of single muscle deformation and that of multiple muscles.....	31
Table 3. Performance of facial expression caused by each type of muscles	32
Table 4. FPS for various facial animations	41

Abstract

In this dissertation, we present physics-based real-time facial animation generated by muscle deformations. Unlike previous muscle-based facial animation using three-dimensional finite elements, we use a two-dimensional shell element to avoid inefficient or undesired tessellations by the thin structure of facial muscles. Instead of a complex continuum shell model dealt with in traditional finite element analysis, we use a geometrically-derived shell model and its energy functions. To accomplish real-time performance, we also adopt modal warping for forwarding time integration of the governing equation.

For the results of facial animation to be anatomically meaningful, our system is designed based on four layers of skin, the subcutaneous layer of flesh, muscles, and the skull with existing knowledge of anatomy. Skin and muscles are composed of shell elements and follow the dynamics of the shell. Subcutaneous fatty tissue is assumed as a uniform elastic body. In principle, facial tissue between the skin and muscle is composed of complex elastic bodies such as the dermis, subcutaneous fat, and fascia. However, we model the layer as a homogeneous deformable-body using a mass-spring system. The fixed part of facial muscles where the muscles originated from the skull is handled by static position constraint.

As facial muscle movements are primarily contraction and relaxation, we control muscle to have stretch deformation using modal analysis. Skin deformation is caused by the force propagation from muscle through subcutaneous fatty tissue. We mimic this phenomenon by applying external force to skin mesh using mass-spring force triggered by muscle deformation. By restricting the region affected by propagated force depending on muscle position, only the region of interest for the skin could be affected by the muscle. For multiple muscles, to prevent the coupling effect between the region of interests, we decouple the system according to the external force type applied to the skin.

We show a series of facial animations caused by selected major muscles that are relevant to expressive skin deformation. Results are affected by muscle-based deformation and indicate

real-time performance. Our system has scalability for importing new types of muscles and skin mesh when their shapes or positions are changed. The system can be used in the field of computer animation and has applications to virtual avatars; it can also be used in the movie and game industries, and it is expected to expand to the medical industry with applications to virtual plastic surgery.

I. Introduction

A. Motivation

The human face provides a variety of types of information, not only from everyday conversations but also from the showing of transformed shapes by internal and external factors caused by aging and/or plastic surgery. Recently, with increasing interest in virtual avatars, the facial animation of humans has been an attractive research topic in various fields from computer graphics to medicine. One of the crucial considerations in creating facial expressions is understanding that they are based on intricate combinations of physiological interactions under the face. This is a challenging problem in that there's no clear definition of classification for facial tissues whose compositions have a high level of complexity [1].

Consequently, the existing method for creating facial animation has been used without considering dynamic properties; these range from handcrafted keyframe animation by artists which are the simplest but the most cumbersome, to approaches using geometric or computer vision-based techniques [2] [3]. For example, the blend shape provides keyframe animation based on geometric deformation and kinematic rigging [4]. This allows for real-time animation; however, it requires extra equipment such as a depth camera and it requires extra attention such as in advance data processing. It also has limitations in applications which require dynamic effects that should observe Newtonian dynamics in VFX films or 3D virtual surgery.

In other respects, physics-based animation for the human face is another branch of facial animation studies. Simulation of the anatomy-based structure of the human face has been developed in computer graphics and biomechanics. In essence, physics-based animations are governed by differential equations satisfying Newtonian dynamics. They also require the use of the simplified anatomical structure of the face; these provide physical interactions between elastic bodies in the face [5], [6]. Though they have anatomically meaningful and visually-compelling results, the simulation performance is rather slow.

Moreover, the problem of tessellations of a thin structure of facial muscles has arisen in previous works due to volumetric analysis [7], [8]. As human body components such as facial muscles and ligaments are thin elastic bodies, they need to be analyzed in different ways. In

biomechanics, simulating a thin ligament of the joint using the Finite Element Method (FEM) Shell Theory for the human body is one method used [9] but it is not a real-time simulation and there are no previous studies that can be used to interpret facial muscles as shells in either computer graphics or biomechanics.

B. Research Goal

The goal of this study is to generate real-time physics-based facial animations with various expressions in an anatomically plausible way. We aim to model human facial anatomy structures with their physical properties and reflect interactions between facial elastic bodies in a dynamic system. Unlike previous works that involved the building of muscles embedded in the soft tissue layer to prevent undesirable tessellations, we construct the thin anatomical structure of a face using shell element analysis so that muscles could be modeled explicitly.

From the perspective of simulation, we consider physics-based simulation for non-linear deformations of the face. To provide simulation in real-time, we adopt the modal warping technique that decomposes total deformation by mode shapes so that the dimension of computation matrices is largely decreased. As facial deformation is a coupled system of multiple muscles and external forces, we mimic various actions of external factors on skin surfaces.

C. Challenges

To imitate coupled non-linear facial deformations, we have to simplify the face model and generate combined facial deformations by analyzing the physical interactions of the given model. However, it is difficult to classify an ambiguous facial system composed of numerous intertwined elastomers which varied from person to person. Also, we have to know where the skin should be deformed or undeformed according to an external force. However, in the coupled system, although the points of action are defined, predefined action points can be destroyed by other definitions. Thus, the main challenges to designing real-time facial animations are as follows:

Modeling perspective: The face is composed of numerous types and number of elastomers. They not only have different geometric and physical properties such as in a material model but they are positioned differently from person to person and change when a face is deformed. Thus, the normalization and simplification of face models to form the base framework of the facial simulation are needed.

Physical interaction perspective: Facial deformation is caused by muscle actuation. However, contrary to body motion which focuses on muscle actuation and corresponding deformation by the kinematic movement of bones, facial motion focuses on skin deformation changed by the deformation of elastic facial muscles. Thus, it is necessary to define how the muscles propagate through the elastomers and exert an external force on the skin as well as where the force is applied to.

Coupled phenomena of facial expressions: Facial expression is the coupled result of multiple interactions among muscles and external forces. Even for a single facial expression, multiple types of muscles work on the same face. To prevent the intertangled effect of multiple external factors, they should be applied independently via decoupling the system.

Real-time integration for non-linear deformation: For non-linear deformation, as the stiffness matrix for the displacement vector is not constant, the numerical time integration for differential equations for motion is a non-trivial problem that results in extensive computational time. The modal warping technique approximates non-linear deformation into combinations of displacements of modal shapes by assuming the stiffness matrix constant.

D. Main Contributions

Thus, our main contributions are as follows:

- **Biomechanical deformation for a face with a novel face model**
- **Real-time simulation for non-linear facial deformation with modal analysis**
- **Approximation of coupled animation with a decoupled system**

First, we model facial muscles and skin by creating a simplified structure including 4 layers under the skin's surface indicating the anatomical composition of the face. We also reflect mechanical interactions between the layers including force propagation and action points of the forces. To prevent undesired mesh generation, we analyze muscles and skin as shell elements, which makes explicit modeling for muscles possible.

To achieve real-time integration for non-linear deformation of the skin surface and muscle objects, by adopting modal warping, the degree-of-freedom (DOF) of the governing equation is considerably decreased so that we could save time in computation. Furthermore, by using modal analysis, the reduced deformation of muscles only for stretch deformation is realized.

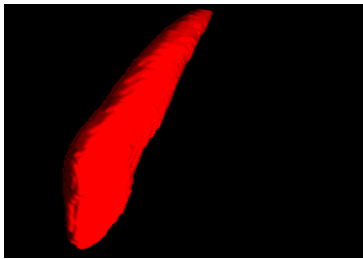
Finally, we decouple the governing equation according to skin deformation type so that multiple muscles affect a single skin surface. After obtaining displacement fields of each external factor independently, by simply doing a summation of them, we could simulate combined skin deformations for each expression.

II. Related Work

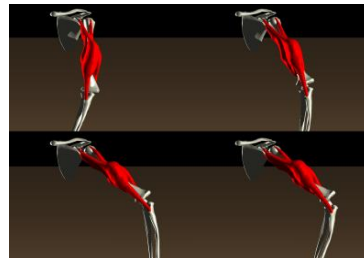
In this study, we surveyed papers for information on muscle-based simulations. We investigated previous works that addressed the simulation of both face and human bodies. We investigated how to model structural geometry and physics of the human muscular system with a special focus on rigging and skinning whose purposes are to connect skin with subcutaneous tissues to design anatomical face models. For facial animation, we also searched for kinematic and dynamic methods to compare their pros and cons.

A. Muscle-based Modeling

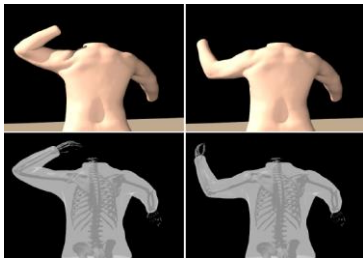
Skeletal muscle-based human body animation using dynamics has been a topic of recent research. Zhu et al. [10] proposed real-time volumetric muscle deformation for the arm using a volume hierarchy model and a FEM with explicit integration. They reconstructed volumetric muscle meshes from CT images and adopted the muscle deformation framework constrained to



(a) Voxel muscle [10]



(b) Skeletal muscle deformation [11]



(c) Flesh simulation by skeleton [12]



(d) Flesh simulation with *Neo-Hookean* [13]

Figure 1. Muscle-based animation for human bodies

the bone. Teran et al. [11] calculated muscle activation corresponding to the skeletal pose by formulating geometrically-designed strain energy using the finite volume method (FVM). By using FVM instead of FEM, they reduced the number of calculated nodes. Teran et al. [12] also developed the quasi-static algorithm for flesh simulation using FEM where hyperelastic material was applied to the volumetric mesh. Smith et al. [13] complemented the works of Teran et al. [12] to accomplish a stable *Neo-Hookean* material model for volumetric flesh. However, [11], [12], and [13] may not be computable in real-time. Besides, facial anatomy was not included among their various considerations.

B. Facial Animation

A muscle-based facial system has been studied for the animation of human expression. For the facial animation in general, there have been two kinds of approaches: These are kinematic-based and physics-based [14].

1. Kinematic Approach

Kinematic approaches are done with the handcrafted method or in general, with the performance-driven method. State-of-the-art. performance-driven animation uses facial tracking algorithms that are based on computer vision. Reed et al. [15] designed user-generated facial animation by sampling the evolutionary framework using genetic algorithms.

Bickel et al. [2] presented multi-scale real-time facial animation that decoupled large deformation and fine deformation processes. For large deformation, they used a marker-based



Figure 2. Multi-scaled facial animation with marker-based motion capture [2]

facial motion capture technique. Then, fine-scale details like wrinkles of the face were generated by linear shell-based mesh deformations including stretch and bending energy with wrinkle geometry through energy optimization. Later, for fine-scale deformation, a data-driven approach was employed for learning fine-scale details from sample poses [16].

Contrary to the works of [2], [16], Weise et al. [3] suggested novel markerless facial tracking methods in a specific environment for real-time facial animation using membrane energy for skin deformation. With facial depth information, a generic template mesh was fitted to the target user's face and tracked offline for training the expression of reconstructed mesh. This study was extended for the general environment except that it used a Kinect sensor and represented facial animation as a weighted sum of blend shape meshes generated in the way of example-based facial rigging. Tracking facial animation data were retargeted to virtual avatars [17]. Li et al. [18] refined the tracking pipeline of [17] for more accurate tracking data. Rhee et al. [19] also implemented markerless real-time facial simulation with tracking; however, they use a single video camera. For reliable facial tracking, they tracked the upper face and the lower face which allowed for local feature tracking of subtle movements and global appearance matching. According to the given tracking data, the face mesh was deformed geometrically using interpolation.



Figure 3. Markerless tracking for real-time facial animation of the virtual avatar using Kinect [17]

Kinematic approaches generally have real-time performance; however, they do not consider anatomical characteristics and dynamics of the human facial system and they are still constrained by the camera used and by handcrafted situations.

2. Facial Rigging

In the absence of facial tracking data or manual adjustments, facial rigging is used to create skin deformations, which is one step closer to reflecting the physical properties of the face. Facial rigging can be implemented in various ways; one of these is by specifying the parameters on skin mesh using the parameters in geometric deformations or using them dynamically [20].

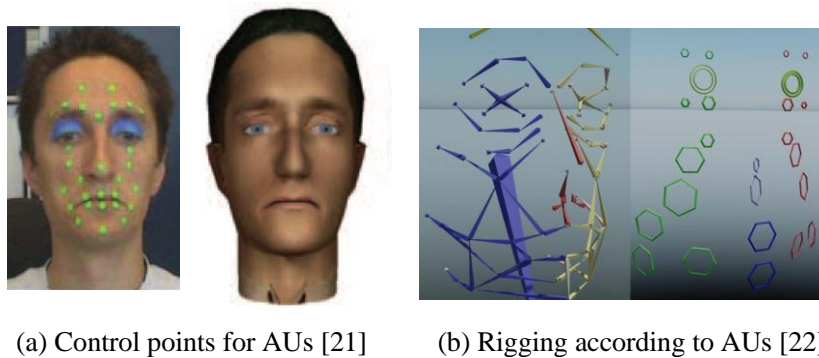


Figure 4. Facial rigging with FACS

Wojdel et al. [21] and Villagrasa et al. [22] developed facial parameters using the facial action coding system (FACS). FACS has action units (AUs) and each unit has its role in modifying the corresponding parts of the skin. While [22] used rigged bones and locators for AU rigging and for setting manual skinning, [21] defined direction vector and density function for each of the AUs to implement skin deformations. They used control points to define the direction and density functions, including predefined landmarks and facial features such as the mouth contour, the eye contour, and the eyebrows. As AUs are not decoupled, they analyzed combinations of AUs to cover the situations involving multiple AUs of the same area of the face.

Komorowski et al. [23] made rigging systems using scattered data interpolation techniques. With given N poses they stored multiple poses and interpolated among them using position constraints. They stored the facial poses, broken down into elementary facial actions, according to the FACS. Using calculated, interpolated data, facial animation was finally created with the blend shape.

For facial rigging, existing anatomical knowledge is included from the perspectives of geometric characteristics. Gao et al. [24] carried out the prediction of muscles when detected

landmarks of the face were given with manually-designed training data. Bibliowicz [25] implemented muscles in the rig with anatomical knowledge of muscle insertions and set them according to the connection of muscles and wires to make deformation sets for each part of facial actions.

However, there is still a lack of anatomical meaning in understanding the geometry of the skin, muscle, and soft tissue layer and the interactions among them. They also have no physics-based deformations for skin and its sub-structures.



(a) Predicted positioned muscles [24] (b) Muscles in rig [25]

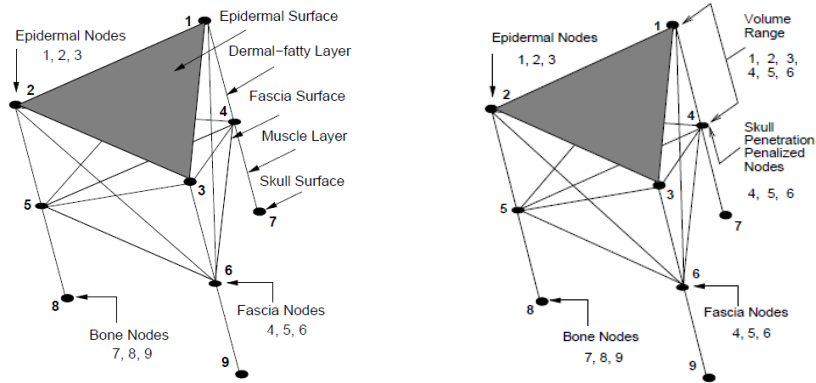
Figure 5. Facial rigging considering muscle positions.

3. Dynamic Approach with Anatomical Properties

To simulate real-world facial motion, the geometric and physical characteristics of facial anatomy need to be considered for modeling facial structures, and deformation of the generated model also needs to follow Newton's second law.

Waters [26] reflected the muscle anatomy of the human face for the facial system. Muscles in this system were modeled as embedded vectors on skin surfaces. Zhang et al. [27] presented a geometrically-formulated, muscle-driven wrinkle model with a physics-based facial animation system that had a hierarchical structure of the skin, muscles, and skull. In this model, the muscle was attached to the skull and inserted into the skin and then represented as a triangular mesh with non-linear springs and deformations under a field of muscle forces. However, they only included the muscle vector field without implementing subcutaneous tissue. With continuum meshing for finite elements (FEs), Pieper et al. [28] considered soft tissue designing surgical simulation using linear FEM. Essa et al. [29] proposed a vision-based, instead of FACS, muscle

actuation system in which they used the method of [28] for muscle and skin attachments; however, muscle actuation was not decoupled.



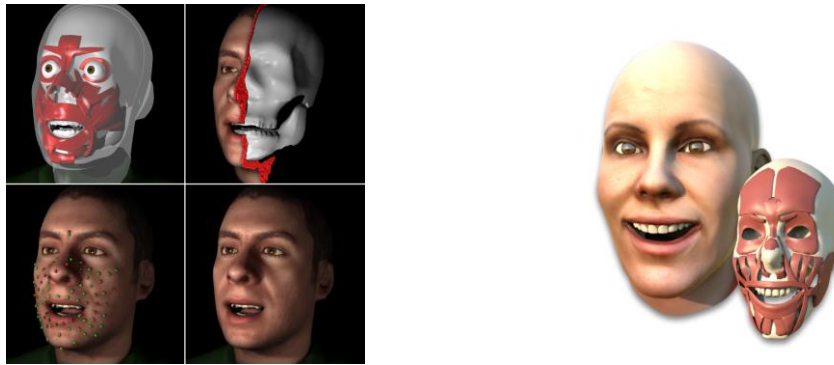
(a) Facial tissue layer [30] (b) Anatomical constraints for face model [31]

Figure 6. Lattice structure mimicking anatomical properties of the face

Terzopolous et al. [30] explicitly designed facial tissue and muscles using deformable lattices constructed from point masses connected by springs that produce real-time performance. Lattices are composed of the epidermal surface, the dermal-fatty layer, the fascia surface, the muscle layer, and the skull surface. For the dermal-fatty layer of [30], Lee et al. [31] added volume preservation forces and skull penetration constraint forces where the face model was governed by Newton's law of motion.

For a more delicate analysis, FEM is used to govern dynamic equations of the face [32]. Gladilin et al. [33] constructed a physiological mechanism for the effect of contracting muscles on soft tissues under the tetrahedral grid. Soft tissue was modeled with *St. Venant-Kirchhoff material* and muscles were represented as a vector field on the skin surface and activated by tangential force. To enforce muscle force in the proper area of the skin, they designated the muscle insertion area as a cone-shaped prolongation of the muscle domain. For multiple muscle actuations, facial expressions were estimated by the superposition of single muscles. Barbarino et al. [5] used FEM with hexahedron elements for each facial layer including the skull and mandibula, muscles, retaining ligaments, skin, and superficial musculoaponeurotic system (SMAS). The hyperelastic model was applied to deformable bodies and interactions among elastic bodies were controlled by a boundary condition.

Wu et al. [6], Sifakis et al. [7], and Ichim et al. [8] used FEM with tetrahedral mesh. They modeled muscles embedded in the tissue layer so that additional rigging was not required. Anatomically-designed layers are described in detail in section IV. Wu et al. [6] applied hyperelastic material and fulfilled heterogeneous material by adjusting the parameters of the material model. For muscle deformation, they defined maximum tension by an experimentally-determined optimal stretch. Unlike Wu et al. [6], Sifakis et al. [7] and Ichim et al. [8] controlled muscle actuation parameters. [7] estimated the muscle activation vector by optimizing the equilibrium position to be given as a target face with markers. Marker positions were compared between the input and the simulation results. [8] calculated muscle activations by solving inverse dynamics that are a constrained optimization form for the given facial expression model generated by a user-specific blend shape.



(a) Anatomical structure for face model (top) and comparison of marker positions (bottom left) and simulation results (bottom right) [7] (b) Muscle activation and corresponding skin deformation [8]

Figure 7. Physics-based facial simulation with an anatomically-designed system

With volumetric FEM, anatomical properties of the face can be applied more elaborately; however, for existing methods, simulation cannot be done in real-time as well as generate unwanted tessellations due to structural characteristics of elements and thin muscle.

Barrielle et al. [34] showed real-time performance using project dynamics with strain energy for skin deformation, but their muscle actuation was based on blend shape which is not physics-based and does not consider the anatomical structure of the face.

III. Real-time Thin Shell Simulation using Modal Warping

For real-time FEM simulation of the thin shell, our governing equation of the face model is largely based on the work of Choi et al. [35]. In this section, for completeness, we shortly describe the derivation of the governing equation in using the energy function based on triangular mesh [35] and modal warping for real-time integration [36].

A. Real-time Thin Shell Simulation

Rather than adopting a complex form in traditional continuum shell models like those involving Classical Plate Theory (CPT) [37] or Koiter's Model [38], Choi et al. [35] used a geometrically-driven energy function for shell elements; this was also proposed by Grinspun et al. [39]. The energy function consists of membrane energy for stretching and shearing and flexural energy for bending. Energy functions are formulated by measuring the difference between the deformed and undeformed states of triangle elements assuming that triangles can have homogeneous deformations.

A designed membrane energy form makes the shell resist deformation. Stretch and shear energy shapes are

$$E_A = \sum_A \frac{(\|A\| - \|\bar{A}\|)^2}{\|\bar{A}\|}, \quad (1)$$

$$E_L = \sum_e \frac{(\|e\| - \|\bar{e}\|)^2}{\|\bar{e}\|}, \quad (2)$$

where $\|A\|$ and $\|\bar{A}\|$ are deformed and undeformed areas of the triangle element and $\|e\|$ and $\|\bar{e}\|$ are the deformed and undeformed lengths of the edge, respectively. Thus E_A is element-based; E_L is the edge-based function for membrane energy. Flexural energy is also an edge-based function described as

$$E_B = \sum_e 3(\theta_e - \bar{\theta}_e)^2 \frac{\|\bar{e}\|}{h_e}, \quad (3)$$

where θ_e and $\bar{\theta}_e$ are the deformed and undeformed dihedral angles of the edge e , respectively; h_e represents the average heights of the two triangles sharing the edge e . Equation (3) was derived using the mean curvature at a point of mesh [39].

The sum of given membrane energy and flexural energy is the total elastic energy of the shell elements:

$$E = k_A E_A + k_L E_L + k_B E_B, \quad (4)$$

where k_A , k_L , and k_B are constant stiffnesses for stretching, shearing and bending motions. Taking the derivative of the elastic energy in terms of nodal displacement leads to an elastic force of elastic potential energy:

$$\frac{\partial E(\mathbf{u})}{\partial \mathbf{u}} = \mathbf{K}(\mathbf{u})\mathbf{u}, \quad (5)$$

where \mathbf{u} is a $3n$ -dimensional vector representing the displacement of $3n$ nodes; $\mathbf{K}(\mathbf{u})$ is a $3n \times 3n$ stiffness matrix. Thus, the governing equation of the shell element is

$$\mathbf{M}\ddot{\mathbf{u}} + \mathbf{C}\dot{\mathbf{u}} + \mathbf{K}(\mathbf{u})\mathbf{u} = \mathbf{F}, \quad (6)$$

where \mathbf{M} is the mass matrix and \mathbf{C} is the damping matrix. Choi et al. [35] used *Rayleigh damping* so that $\mathbf{C} = \xi\mathbf{M} + \zeta\mathbf{K}$. \mathbf{F} is a $3n$ -dimensional vector of external forces applied to n nodes.

Choi et al. [35] also presented a novel rotational component based on the Jacobian of triangle orientation. As Choi et al. [36] dealt with tetrahedron meshes, the rotational part was modified for shell elements. As our main focus is not on the formulation of rotation, we refer readers to the work of [35] for further details.

B. Modal Warping

For real-time integration, the governing equation is solved based on modal warping. To apply modal analysis, $\mathbf{K}(\mathbf{u})$ in equation (6) is linearized as a constant matrix \mathbf{K} with a small rotation:

$$\mathbf{M}\ddot{\mathbf{u}} + \mathbf{C}\dot{\mathbf{u}} + \mathbf{K}\mathbf{u} = \mathbf{F}. \quad (7)$$

Then equation (7) could be decoupled with generalized eigenproblem:

$$\begin{aligned} & \text{Find } \Phi, \Lambda \text{ s.t.} \\ & \Phi^T \mathbf{M} \Phi = \mathbf{I}, \quad \Phi^T \mathbf{K} \Phi = \Lambda \text{ where } \mathbf{K} \Phi = \mathbf{M} \Phi \Lambda. \end{aligned} \quad (8)$$

Solutions of general eigenproblem mean that Λ is a diagonal matrix whose components are eigenvalues and columns of matrix Φ are the corresponding eigenvector. Thus, the displacement vector in equation (7) can be represented as

$$\mathbf{u}(t) = \Phi \mathbf{q}(t). \quad (9)$$

Here, Φ is a modal displacement matrix whose columns correspond to the mode shape and $\mathbf{q}(t)$ is a vector whose elements correspond to modal amplitudes. By selecting the number of dominant eigenvalues, the amount of computation is reduced. In equation (9), as the displacement vector and modal amplitude vector are time-dependent, they can be represented as a function of time t .

With modal analysis, the governing equation can be decoupled by the modes. With an assumption of fine mesh and stiffness warping, equation (7) can be represented using local displacement. By multiplying \mathbf{R}^T with both sides of the equation (7) and applying equation (9) to the results, the final shape of the governing equation for the shell element is

$$\mathbf{M}_q \ddot{\mathbf{q}} + \mathbf{C}_q \dot{\mathbf{q}} + \mathbf{K}_q \mathbf{q} = \Phi^T (\mathbf{R}^T \mathbf{F}), \quad (10)$$

where \mathbf{M}_q , \mathbf{C}_q , and \mathbf{K}_q are the matrices of \mathbf{M} , \mathbf{C} , and \mathbf{K} multiplied with Φ^T on the left side and Φ on the right side. Here, \mathbf{q} is the modal amplitude vector for local displacement vector and \mathbf{R}^T is the rotation matrix representing the local coordinate orientation of the nodes. Finally, by solving equation (10) with semi-implicit integration and then calculating \mathbf{u} using equation (9), we were able to simulate given shell elements. Modal amplitudes and the rotation matrix were computed in every frame whereas the matrices of equation (10) were precomputed before the simulation.

IV. Muscle-based Face Model

A. Simplified Design of Anatomical Structure

Facial tissue has a complex structure located within the space between the skin and skull [40], [41] (Figure 8. (a)). However, for the sake of computational plausibility for simulation, we designed a simplified face model. We referred to [5], [6], [30] and for an anatomical background of facial tissue to build a face model.

Facial skin is composed of the epidermis and dermal layers [30], [42]. For the face, the skull acts as a fixed point of muscle origin and supports the whole face model [5]. The space between the skin and skull is composed of different elastic bodies such as subcutaneous fatty tissue, fascia, SMAS, connective tissue, the and gliding plane, etc. Skin deformation is the result of interactions between the elastic bodies and the deformed muscles.

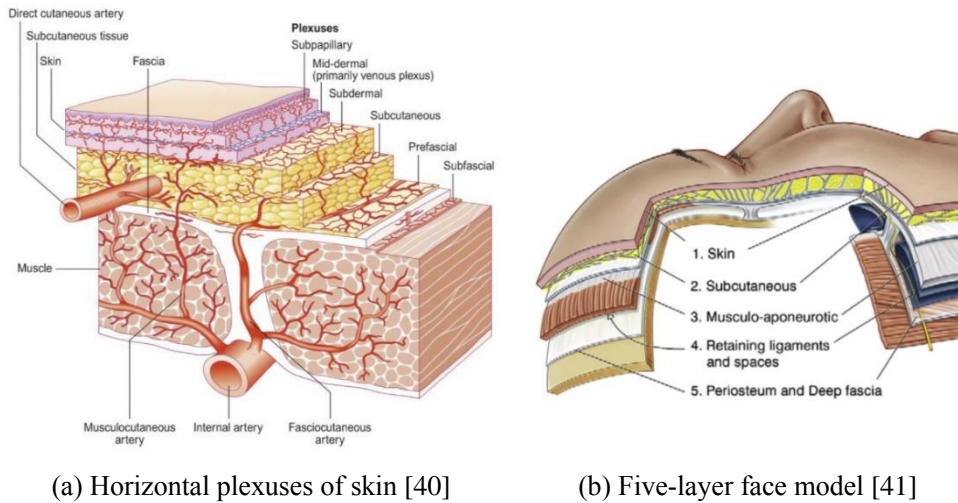


Figure 8. The anatomical structure of the face

Prior works involving facial animation generally have more than 4 layers for each face model. Terzopoulos et al. [30] modeled muscle, fascia, the subcutaneous fatty layer, and the skin using deformable lattices. The anatomical models of Sifakis et al. [7] and Ichim et al. [8] included skull, flesh, muscle, and skin. Wu et al. [6] used a generalized five-layer model (Figure 8. (b))

for the face. Mendelson et al. [41] included skin, subcutaneous tissue, SMAS, a gliding plane, and deep fascia while assuming skin, subcutaneous tissue, and SMAS as a single entity. Deformable bodies of their system were based on tetrahedrons generated by given skin mesh; muscles were embedded in the deformable continuum for the thin structure of facial muscle.

We simplified the anatomical structure including the skull, muscle, subcutaneous fatty layer, and skin similar to the works of [7] and [8]. However, to avoid unintended tessellations and to achieve real-time simulation, we modeled skin and muscle as a plate-shaped elastic body using a shell element. For other deformable bodies, we considered them as a homogeneous single elastic body moving together within the subcutaneous layer. Among existing deformable simulation methods, we selected the mass-spring system to implement anatomical interaction between muscle and skin (Figure 9).

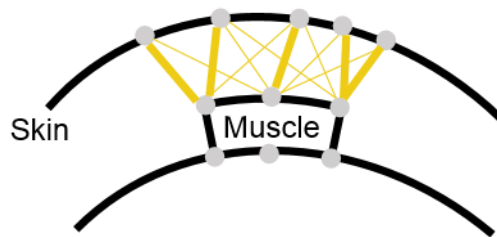


Figure 9. Simplified structure of a face model

To constitute the subcutaneous layer with the mass-spring system, we built a connection using a spring between the skin and muscle nodes. Given positioned muscles inside the skin, muscle nodes are connected to skin nodes that keep the minimum distance to themselves (bold yellow lines of Figure 9). Through connected springs, skin deformation is triggered by muscle. In the case of the skull, we only reflected its role as the anchoring point of the muscle's origin and skin by enforcing constraints.

B. 3D Modeling for Physics-based Facial System

For skin mesh, we obtained a symmetric template quad mesh from FaceShift¹ in .obj file format. Based on J. Rohen's work, Color Atlas of Anatomy [43] and [44], [45], we built facial muscle with given a skin and skull mesh using a modeling tool in Maya. Generally, in anatomy textbooks, the shape and position of the insertions of muscle are considered [5]; and we modeled muscle meshes manually in the form of a curved thin shell and positioned them under the skin mesh (Figure 10). By avoiding muscles that have a negligible influence on the mechanical behavior of skin [5], 4 major muscles were selected to derive large deformation of the skin. Selected muscles include the zygomaticus major for lifting the angle of the mouth; the corrugator supercilii for pulling eyebrows; the depressor labii inferioris for pulling lower lip downward; and the depressor anguli oris for pulling the angle of the mouth downward. For anatomical knowledge of these muscles (like origin, insertion, and action), we referred to ANATOMY NEXT². For the 4 selected major muscles, we have 8 muscles by making the left and right muscles symmetrical with respect to the center of the face. As muscle modeling is done in an independent layer from the skin, if the muscles are modified, they can be removed and imported freely. This scalability is also valid for skin mesh, for example, when simulating with someone else's face mesh.

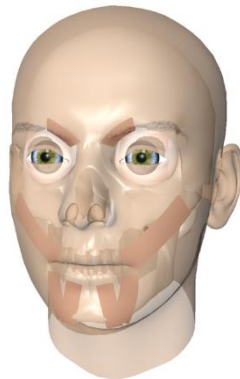


Figure 10. Muscle mesh modeled and positioned with template skin and skull mesh

¹ www.faceshift.com

² www.anatomynext.com

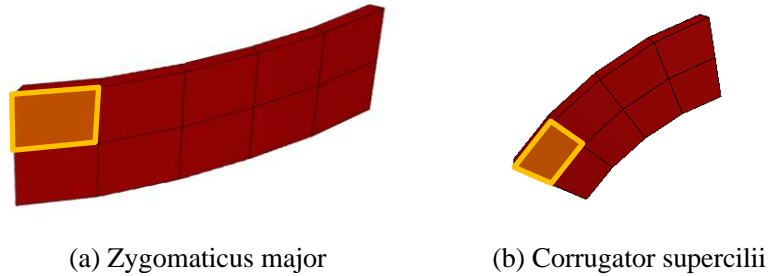


Figure 11. Tessellation of muscle mesh

We set up muscle mesh nodes so that elements in the wide face of muscle objects conform to a square shape. Muscle meshes were modeled with polygonal mesh in Maya that could be exported as in .obj file format. For applying the finite shell element method of Choi et al. [35] to the skin and muscle object, we needed to triangulate the given quad meshes. Since we handled mesh data as an .obj file, getting triangular elements for the stretch energy is easy, but for edge-based shear and flexural energy, we needed to extract edge information separately. After extraction for the element and the edge, we were able to get the number of triangular elements and edges as well as vertex indices for the elements and the edges. See Appendix I for the detailed procedure. Given the configuration of shell elements, skin deforms according to the designed face model.

V. Physics for Face Model

In this section, we explain how to perform forward dynamics in the face model described in section IV. We reflect the following dynamic characteristics: First, muscles undergo stretch deformation by activation force. This leads to spring displacement that connects muscle and skin. Finally, mass-spring force is generated and acts as an external force for skin deformation.

A. Muscle Deformation Control

When facial expressions are created, facial muscles contract or relax while their points of origin are fixed to the skull. In this section, we explain how to mimic those movements using modal analysis, tangential force and static position constraints of shell elements.

Modal analysis

To make shell elements of muscle that have stretch deformation only, we need to find the eigenvector $\mathbf{e}_i \in \mathbb{R}^{3n \times 1}$ that corresponds to $\lambda_i \in \mathbb{R}$ where $n \in \mathbb{R}$ is the number of nodes; $i \in \mathbb{Z}^+$ represents the index of the stretch mode; and λ_i is the solution of the generalized eigenproblem (equation (8)). We have 4 modes and among them, the stretch mode is third which means $i = 3$. Given the modal displacement matrix $\Phi \in \mathbb{R}^{3n \times d}$ where $d \in \mathbb{R}$ is the number of modes, by setting Φ as zero except for \mathbf{e}_i , the displacement of each muscle node becomes the linear combination of the stretch mode shape and its modal amplitude \mathbf{q} . In this case, we have $d = 4$ which is enough to cover bending (12).

$$\mathbf{u} = \Phi \mathbf{q} \tag{11}$$

$$= \begin{pmatrix} 0 & 0 & e_{3_{1x}} & 0 \\ & & e_{3_{1y}} & \\ \vdots & \vdots & \vdots & \vdots \\ & & e_{3_{ny}} & \\ 0 & 0 & e_{3_{nz}} & 0 \end{pmatrix} \mathbf{q}. \tag{12}$$

Finally, DOFs of muscle deformation is constrained for stretch.

Activation force for muscle

When muscles contract and relax, the activation force is needed to trigger muscle movement. As the type of force for those deformations is a compressive or tensile force, we enforce tangential force to the muscle. As our work is based on finite element, the force needs to be exerted as a nodal force to the nodes that are lying at the center of the muscle object (Figure 12). The magnitude of the body force was set manually and the force applied to each node acted as an external force that generates muscle deformation. Thus, the governing equation for muscle is

$$\mathbf{M}_{\mathbf{q}_m} \ddot{\mathbf{q}}_m + \mathbf{C}_{\mathbf{q}_m} \dot{\mathbf{q}}_m + \mathbf{K}_{\mathbf{q}_m} \mathbf{q}_m = \Phi_m^T (\mathbf{R}_m^T \mathbf{F}_{ext_m}), \quad (13)$$

where \mathbf{R}_m is the rotation matrix for the muscle and \mathbf{q}_m , \mathbf{F}_{ext_m} , and Φ_m is the modal amplitude, modal force vector, and modal displacement matrix of the muscle. $\mathbf{M}_{\mathbf{q}_m}$, $\mathbf{C}_{\mathbf{q}_m}$, and $\mathbf{K}_{\mathbf{q}_m}$ are calculated in the same way in equation (10) with the mass, damping, and stiffness matrix of the muscle. By integrating equation (13) with a rotational part of the muscle, we were able to get a displacement field of corresponding muscle, \mathbf{u}_m . The displacements trigger the spring force of the subcutaneous layer in section V.B. We can control muscle deformation in contraction and relaxation by setting the direction of the applied tangential force before starting the simulation.

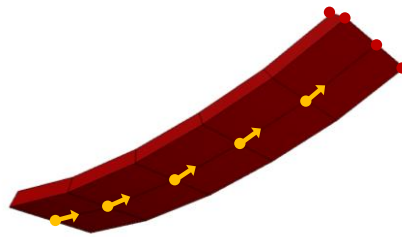


Figure 12. Constrained and enforced muscle nodes

Static position constraints

To fix the end of muscle where it stems from the skull, we enforced static position constraints described in modal warping. By neglecting the corresponding DOFs of the governing equation, nodes that were set to be in the static position has zero displacements. Nodes marked as red in Figure 12 represent the fixed position. This is especially important because in reality muscle pulls the skin toward the skull where it originates from; we enforced contraction force towards static constraints.

B. Force Propagation through the Subcutaneous Layer to the Skin

As muscle and skin are connected by a spring, if one side of the spring moves according to muscle deformation, the other end moves with it. This leads to the spring force of the subcutaneous layer and the spring force is passed to the skin because the other end of spring is attached to the skin node. Transferred force should be applied to the proper skin area around the skin that is connected to the muscle. This area is referred to as a region of interest (ROI).

Mass-spring force

To define mass-spring force [46] of the subcutaneous layer, we called the deformed spring vector, undeformed spring vector, and initial spring vector as \mathbf{S}_d , \mathbf{S}_{ud} , and \mathbf{S}_{init} , respectively. The magnitude of the deformed spring force is

$$|\mathbf{F}_{spring}| = k_{spring} \cdot |\Delta\mathbf{x}| \quad (14)$$

$$= k_{spring} \cdot \frac{||\mathbf{S}_d| - |\mathbf{S}_{init}||}{|\mathbf{S}_{init}|}, \quad (15)$$

where $\Delta\mathbf{x}$ is the relative elongation of the spring to make the spring force proportional to the deformed length difference based on the initial length [46]. Besides, as skin deformation arise along with the direction of muscle movement, the direction of \mathbf{F}_{spring} becomes

$$\frac{\mathbf{S}_d - \mathbf{S}_{ud}}{\|\mathbf{S}_d - \mathbf{S}_{ud}\|} \text{ (Figure 13)}. \quad (16)$$

The governing equation for shell elements for the skin mesh due to muscle-based force becomes

$$\mathbf{M}_{\mathbf{q}_s} \ddot{\mathbf{q}}_s + \mathbf{C}_{\mathbf{q}_s} \dot{\mathbf{q}}_s + \mathbf{K}_{\mathbf{q}_s} \mathbf{q}_s = \Phi_s^T (\mathbf{R}_s^T \mathbf{F}_{ext_s}) \quad (17)$$

$$= \Phi_s^T (\mathbf{R}_s^T \mathbf{F}_{spring}). \quad (18)$$

\mathbf{F}_{spring} is applied only to the skin nodes that are connected with muscle. In this case, \mathbf{F}_{spring} acts as \mathbf{F}_{ext_s} . Other matrices and vectors in equation (17) are calculated for the skin in the same way in equation (13). Using equation (18) with modal warping, we calculated the displacement field of skin, \mathbf{u}_s , deformed by muscle deformation.

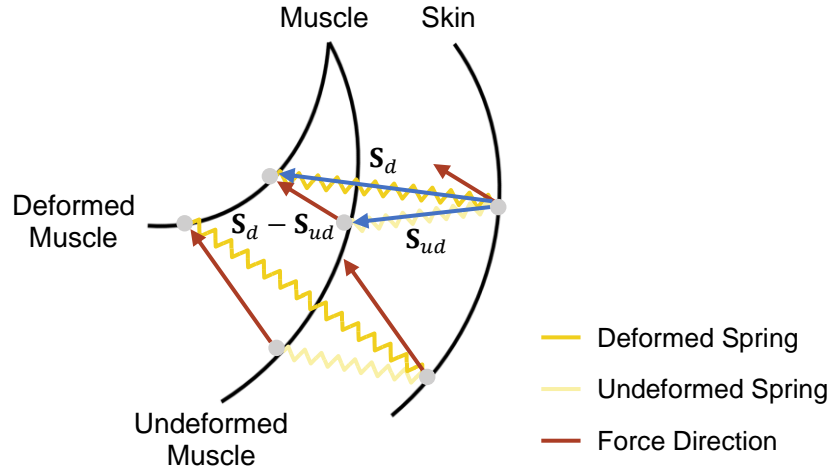


Figure 13. Mass-spring force direction according to muscle and skin attached to it

Spring vectors are relative vectors between the skin and the deformed muscle or skin and undeformed muscle vertices. As the deformed muscle vertex includes \mathbf{u}_m caused by muscle deformation, we can say that force generated by muscle deformation is propagated through the subcutaneous spring layer.

Region of Interest (ROI)

Although \mathbf{F}_{spring} was applied to specific nodes, it could have affected the undesired region of the face. However, in reality, muscle does not affect the skin area except around the region where it is positioned; for instance, the forehead is not affected by the muscle that pulls down the angle of the mouth. To prevent such undesired influences, we limited the area where skin can be deformed. The area around the skin connected with muscle is called a region of interest (ROI). We restricted the DOFs of skin nodes that are in the non-ROI by applying the static position constraint. The criteria for selecting skin nodes corresponding to the ROI are as follows:

Let \mathbb{M}_x , \mathbb{S} as a set of node indices in muscle x and skin mesh while m_i , s_j represent the i -th node of muscle x and j -th node of skin, respectively. Also, let \mathbb{I}_x be a set of nodes in an ROI of muscle x and $\mathbf{S}_{init}^{x_i}$ as an initial undeformed spring between the i -th node of muscle x and the skin node connected with it. The ROI can be defined as:

$$\begin{aligned} & s_j \in \mathbb{I}_x \quad s. t. \\ \exists_{i,j}, \quad & \alpha \cdot |\mathbf{S}_{init}^{x_i}| > |m_i - s_j| \quad \text{where } i \in \mathbb{M}_x, j \in \mathbb{S}. \end{aligned} \quad (19)$$

Here, α is a parameter for determining a range of ROI for muscle x . ROIs for modeled muscles were precomputed. Given the nodes in \mathbb{I}_x , by setting static constraints for the non-ROI, the nodes of non-interest are reduced in the governing equation.

VI. Force Decomposition for Combined Facial Deformation

Although we restricted ROIs according to muscle type, for a single system, ROIs could be overlapped for different muscles. Also, since we set a fixed point of skin differently according to an external factor, the ROI defined for the muscle could be distorted if an external force such as gravity is applied to the skin. To keep ROIs independent of different muscles and external forces, we decomposed the system by the type of external force that induces skin deformation. For $i \in \{1, \dots, k\}$ and $j \in \{1, \dots, l\}$, $k \in \mathbb{Z}^+$ and $l \in \mathbb{Z}^+$ means the index number of different muscles and different external forces such as gravity except caused by muscle. Given the external force \mathbf{F}_{ext_s} in governing equation (17), \mathbf{F}_{ext_s} is represented as

$$\mathbf{F}_{ext_s} = \mathbf{F}_{M_1} + \mathbf{F}_{M_2} + \dots + \mathbf{F}_{M_k} + \mathbf{F}_{ext_{s_1}} + \mathbf{F}_{ext_{s_2}} + \dots + \mathbf{F}_{ext_{s_l}}, \quad (20)$$

where \mathbf{F}_{M_i} is an external spring force caused by the i -th muscle and $\mathbf{F}_{ext_{s_j}}$ is a j -th external non-muscle force. Thus, equation (20) implies that \mathbf{F}_{ext_s} can be decomposed into the sum of external forces generated by k muscles and l different kinds of external non-muscle forces.

With equation (20), the governing equation for skin deformation equation (17) can be decomposed depending on different external forces (see Appendix II). This means the system can be decoupled according to the type of deformation. Thus, we can say that

$$\mathbf{u}_s = \sum_f \mathbf{u}_f, \quad (21)$$

where $f \in \{M_i, ext_{s_j}\}$ is representative of force type and \mathbf{u}_f is representative of the displacement field of the skin due to the i -th muscle or the j -th external force. By calculating \mathbf{u}_f respectively according to types of external force, ROI for any external force is respected. In other words, for example, the skin area around the lips is only affected by the muscles

working for the lips and another external force like gravity can affect the area independently.

In the decoupled system, to compute \mathbf{u}_f respectively, we need the corresponding number of skin meshes and have to simulate the meshes according to the given external force. After the independent process, by simple summation for calculated displacement fields, the total displacement field of the skin is integrated (Figure 14).

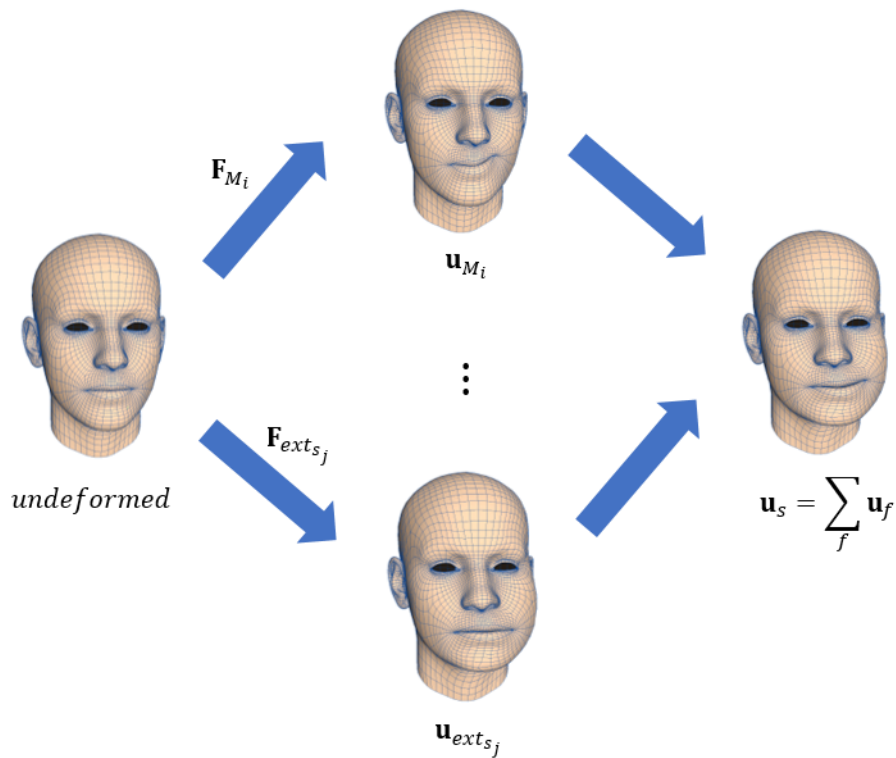


Figure 14. Decoupling and integrating the displacement field of skin mesh

VII. Experimental Results

The simulation results of the suggested algorithm for facial simulation are described in this section. We validated each component of the algorithm by showing the results of skin and muscle deformation mainly focused on the skin.

A. Implementation Details

We developed our facial animation system for Maya 2017 plugin based on C++ programming language and we used Maya script language MEL, Maya plugin API for C++ language³ and C++ language-based FEM simulation framework of [35]. Our programs ran on 3.6GHz 8-Core Intel(R) Core(TM) i7-4790 CPU and NVIDIA TITAN Xp with 16GB RAM under Windows 8.

Maya plug-in structure

The plug-in is the core brain of our simulation that plays the role of solving governing equations. Input and output mesh for the plug-in is modeled and stored in Maya. Input polygon meshes are transferred to our plug-in as initial meshes of simulation and the vertex position of output polygon meshes are changed by calculations defined in the plug-in.

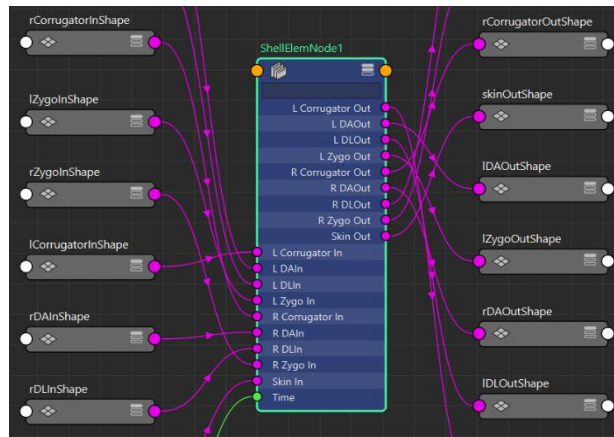


Figure 15. Plug-in and the connections with input and output mesh

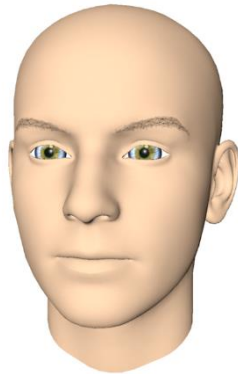
³ <http://help.autodesk.com/view/MAYAUL/2017/ENU/>

B. Mesh Generation

Meshes for skin and muscles were modeled as shown in Figure 16. According to section IV.B., skin mesh was obtained; it has 7366 nodes and muscle meshes consisting of 36 nodes except for the corrugator supercilii muscle that has 30 nodes. After extracting the element and the edge, we have 14,600 elements and 21,968 edges for the skin and 68 elements and 102 edges for the muscles except for the corrugator supercilii that has 56 elements and 84 edges.

Table 1. Number# of nodes, elements, and edges for simulation meshes

Mesh Type	Node	Element	Edge
Skin	7,366	14,600	21,968
Zygomaticus major	36	68	102
Corrugator supercilii	30	56	84
Depressor labii inferioris	36	68	102
Depressor anguli oris	36	68	102



(a) Neutral face: Initial state



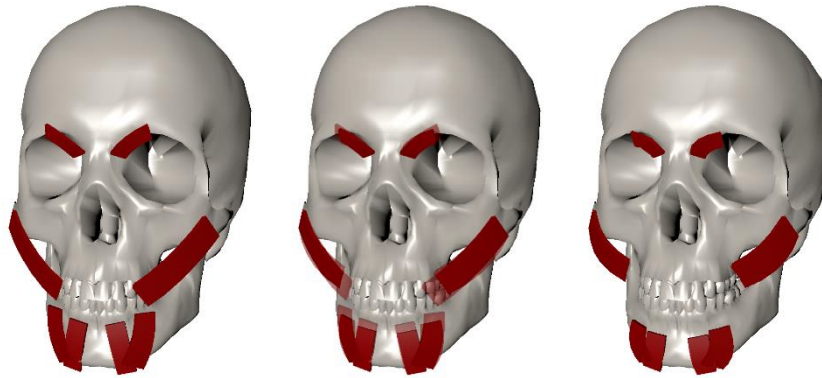
(b) Initial state of muscles

Figure 16. Skin, muscle, and skull mesh for face model

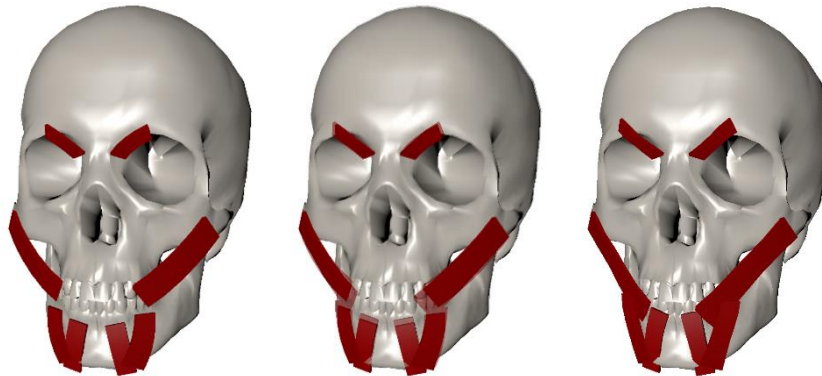
C. Simulation Results

1. Muscle Deformation

Figure 17 shows muscle deformation of the zygomaticus major, the corrugator supercillii, the depressor labii inferioris, and the depressor anguli oris, where 8 muscles deformed simultaneously. Muscles were constrained by static constraints for the end of the muscle where the muscle originates from the skull. By changing the direction of the applied tangential force, we were able to control the contraction and expansion of the muscle.



(a) Muscle contraction from an undeformed state (left to right)



(b) Muscle relaxation from an undeformed state (left to right)

Figure 17. Muscle deformation by external tangential force with static constraint points

Table 2. Simulation performance of single muscle deformation and that of multiple muscles

	Single muscle				Multiple muscles
	Zygomaticus major	Corrugator supercillii	Depressor labii inferioris	Depressor anguli oris	All 8 muscles
FPS	220	210	210	210	200

Compelling results of muscle contraction and relaxation shown in Figure 17 imply that modal analysis for muscles with stretch deformation achieved a reliable value. The results in Table 2 show real-time performance for muscle deformations.

2. Skin Deformation

For skin deformation, we validated that the proposed anatomical design for the facial model and the interaction between its elastic bodies works well while assuming that skin deformation is created by muscle deformation; this justified the assertion that muscle deformation should have been preceded by skin deformation. We mainly present skin deformation according to the ROI and show utilities of the force decomposition.

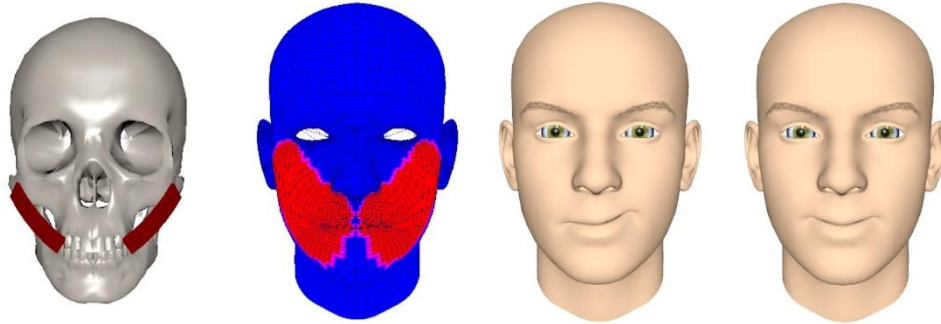
Region of Interest (ROI)

Figure 18, Figure 19, and Figure 20 demonstrate that the proposed ROI method works well and that the muscles were properly positioned. The second column of Figure 18 shows an ROI generated by muscle given in the first column of Figure 18. The blue area of the ROI represents statically-constrained points and the red area is deformed by muscle. We first confirmed the results of the skin deformations due to the single type of muscle for the three types of muscles except for corrugator supercillii. For each type, the skin surface was deformed by the right side muscle only and then by both sides (third and fourth columns of Figure 18). For the corrugator supercillii muscle, which pulls the area around the eyebrows up and down as it deforms, it generates delicate deformations of the skin; we controlled both sides of the muscle contraction and relaxation and show the results in more detail (Figure 20). The results illustrated in Figure

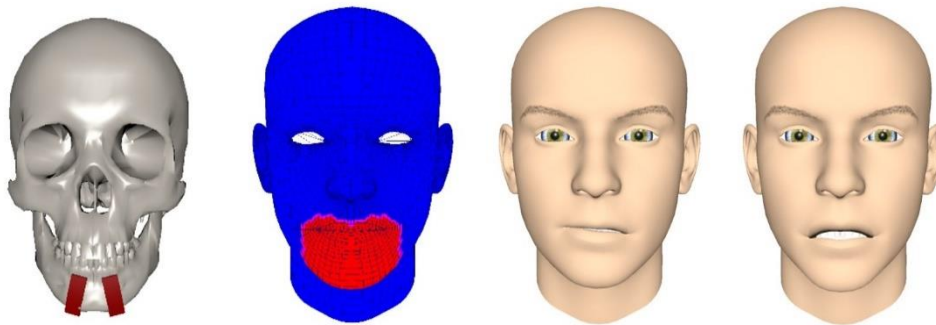
20 were achieved with muscle mesh for corrugator supercilii and corresponding ROI (Figure 19). All results strongly indicate real-time performance (see Table 3).

Table 3. Performance of facial expression caused by each type of muscles

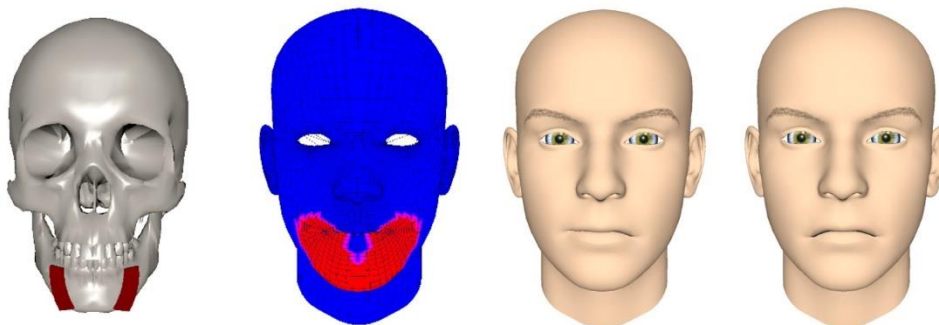
Muscle type	Zygomaticus major		Corrugator supercilii		Depressor labii inferioris		Depressor anguli oris	
	Right side only	Both sides	Right side only	Both sides	Right side only	Both sides	Right side only	Both sides
FPS	95	90	97	93	95	90	96	96



(a) Zygomaticus major

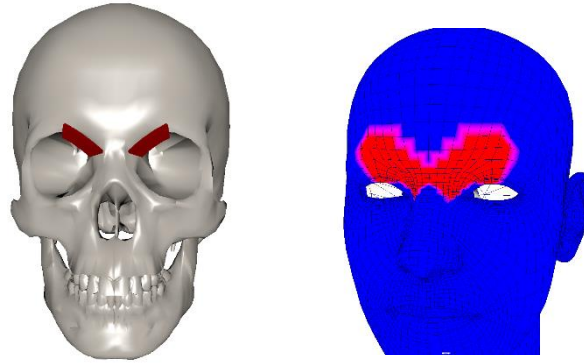


(b) Depressor labii inferioris



(c) Depressor anguli oris

Figure 18. Facial muscle, corresponding ROI, and skin deformation due to the contraction of the right muscle and both the left and right muscles (left to right for each row)



(a) Corrugator supercilii (b) ROI of (a)

Figure 19. Insertion and ROI of corrugator supercilii

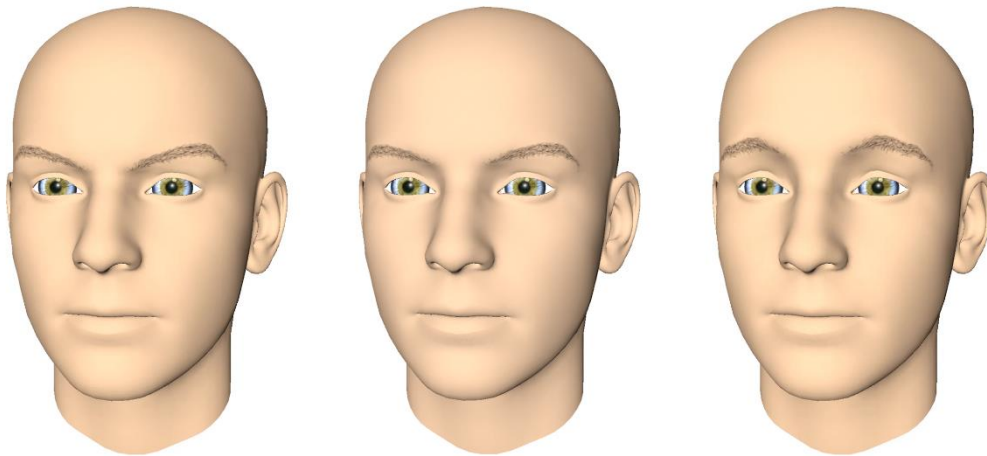


Figure 20. Skin deformation due to contraction (center to left) and relaxation (center to right) of corrugator supercilii from the neutral face (center)

Gravity load

We also tested skin deformation by external forces other than those produced by the muscle. We employed gravity force to simulate dynamic effects on the skin and to exert static constraints to the positions to fix and anchor the skin to the skull. The backside of the head and feature points of the face were fixed. Figure 21 shows the constrained part of the skin (blue) and unconstrained (red) vertices. In Figure 21, vertices marked with yellow were also fixed feature points. For the same gravity load, we simulated shell elements of the skin's surface with different stiffnesses. Figure 22 illustrates that as stiffness decreased under the same gravity, the degree of skin sagging increased near the eyes and under the cheeks. The simulation performance with gravity was about 85 Fame Per Second (FPS).

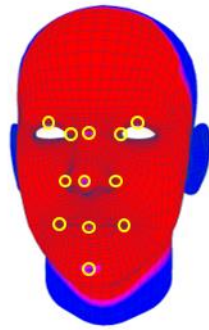


Figure 21. Static constraints of skin for gravity load

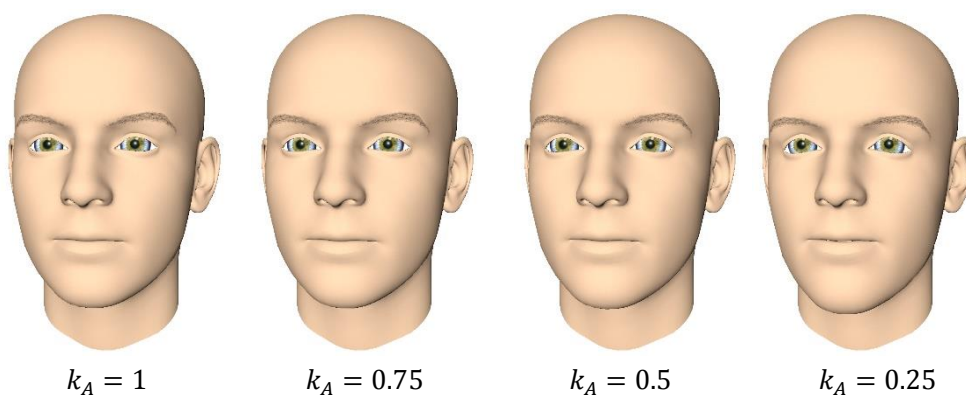


Figure 22. Gravity load for skin with decreasing element stiffnesses

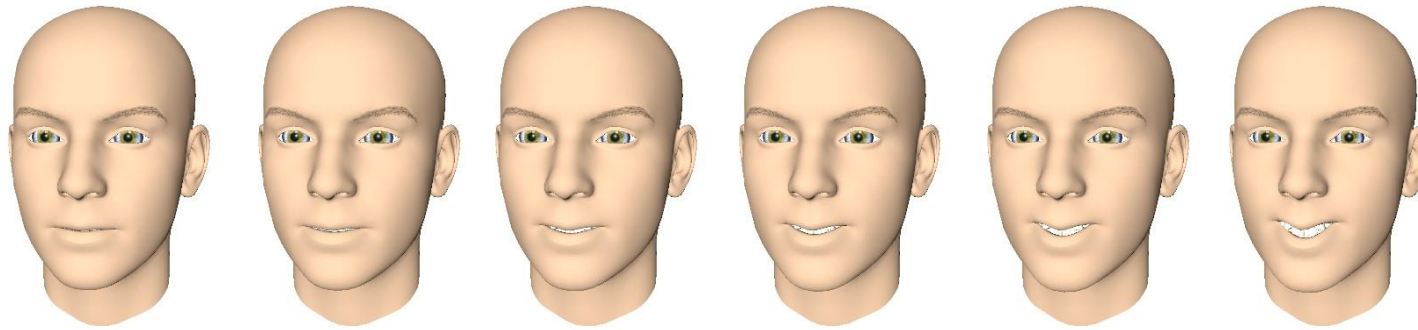
Force decomposition

To validate that skin deformation by force decomposition is reliable, we show a series of animations. First, we demonstrate skin deformation with concurrent deformations of multiple muscles. Also, we show that the deformation caused by the external forces applied to the skin is expressed as $\mathbf{F}_{ext_{s_1}}$, pulling the right cheek and causing muscle contraction.

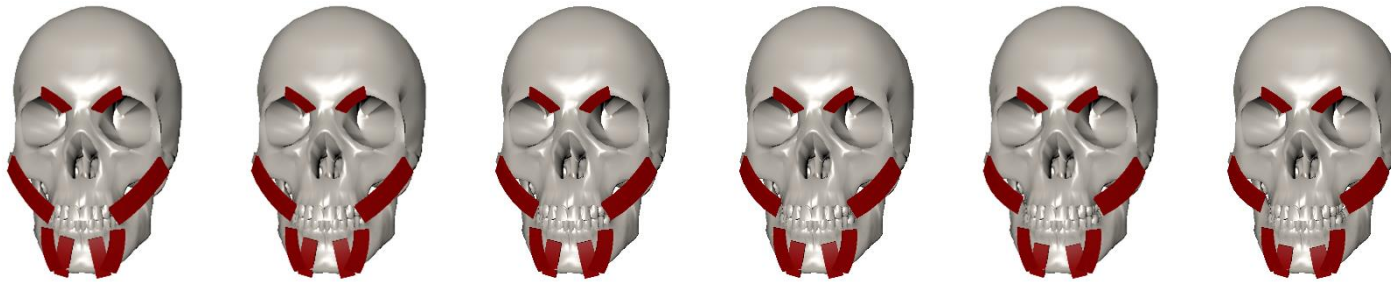
For multiple muscles, we enforced the contraction force to the zygomaticus major and depressor labii inferioris concurrently. Each displacement field was the same as the result of Figure 18 deformed by the ROI and muscle of Figure 18. The results of integrated displacement fields are shown in Figure 23. By affecting the zygomaticus major, which lifts the oral angle, and the depressor labii inferioris, that pulls the lower lip down, the lower lip was opened and made to smile. Deformations of muscles that move concurrently under the skin could also be seen (Figure 23). In terms of performance, multiple muscle animations had 82 FPS.

Zygomaticus major was also chosen as the muscle where the $\mathbf{F}_{ext_{s_1}}$ and the muscle force interacted with the skin at the same time. The static constraints (blue area and marked yellow) for the dragging force and its corresponding displacement field are shown in Figure 24. The result of adding two displacement fields for a given situation is shown in Figure 25. The animation of the mouth rising upward as the right cheek stretched as shown in Figure 25, had 73 FPS.

Results of Figure 23 and Figure 25 show that the simulation results by using the displacement field obtained from the force decomposition system were appropriate and effective. Furthermore, more muscles acting on the skin or other external forces can be easily implemented by the decoupled system.

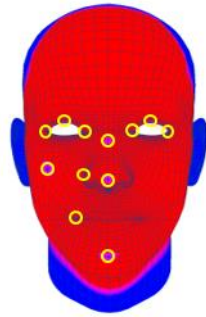


(a) Skin deformation due to combined displacement fields

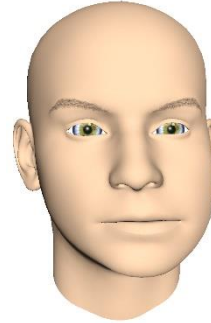


(b) Simultaneous contraction of zygomaticus major and depressor labii inferioris

Figure 23. Frame by frame animation for simultaneous deformation of multiple muscles causing combined skin deformation



(a) Static points of $\mathbf{F}_{ext_{s_1}}$



(b) Displacement field $\mathbf{u}_{ext_{s_1}}$ of $\mathbf{F}_{ext_{s_1}}$

Figure 24. Static constraints and corresponding displacement field of $\mathbf{F}_{ext_{s_1}}$

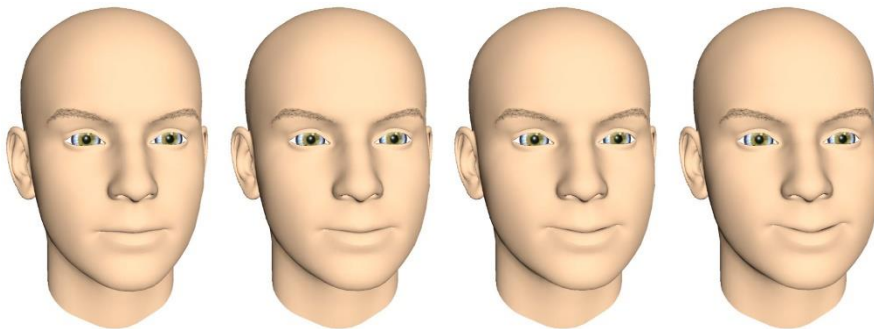


Figure 25. Skin deformation caused by concurrent effects by $\mathbf{F}_{ext_{s_1}}$ and contraction of zygomaticus major

Transition

Thanks to the force decomposition system, various expressions can be realized in our system. We present transitions between different facial expressions going through a neutral face. The facial transition was completed with only dynamic control, contraction, and relaxation of muscles, with no need for any geometric interpolations. During the simulation, displacement fields of the zygomaticus major and depressor anguli oris were calculated independently along with related muscle deformation. Thus, each ROI was transformed independently so that displacements of different areas were added together and the transition was automatically accomplished.

Figure 26 illustrates, in detail, the transition results over time. During the simulation, the displacement fields for the muscle and that region of interest were continually calculated. For all time domains, the external force could be applied to a specific muscle. From t_0 to t_1 , the zygomaticus major was engaged by tangential force to contract, so that the skin surface near the oral angle was lifted. After t_1 , the zygomaticus major is relaxed, which means that the external force direction was changed to the opposite. Consequently, the muscle started to expand and simultaneously the lifted oral angle fell as the muscle relaxed until t_2 . At the last time interval, from t_2 to t_3 , tangential force for the zygomaticus major was removed and the depressor anguli oris was forced to contract.

Scalability

With a slight modification of the muscle's position and orientation under the given skin surface, applying our system to a user-specific facial model can be done easily. User-specific skin mesh is obtained in the same way with FaceShift having the same number of nodes, elements, and edges of template skin mesh. We demonstrated facial simulations deformed by the zygomaticus major and the depressor anguli oris and then combined skin deformations due to the zygomaticus major and the depressor labii inferioris.

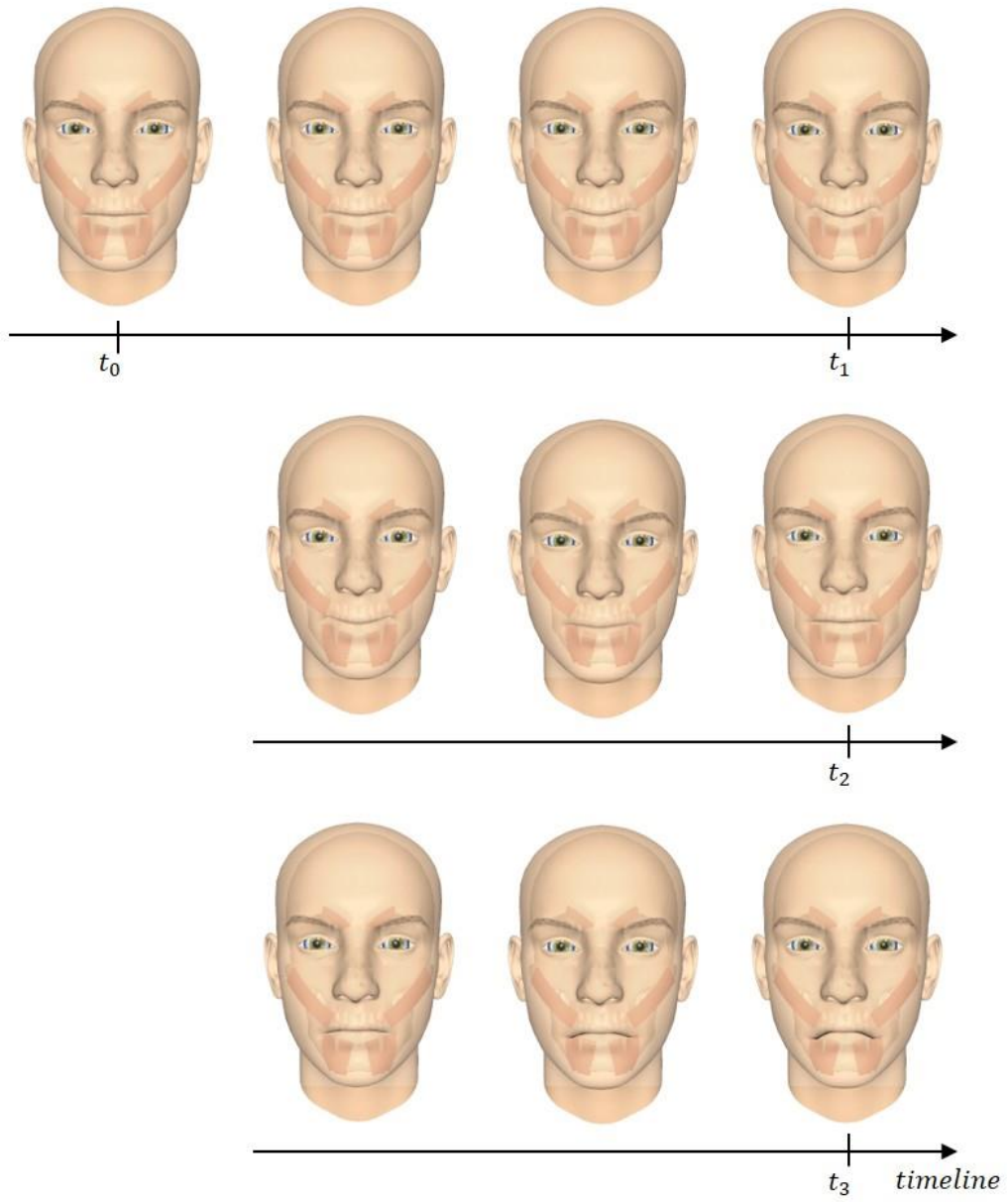


Figure 26. Transition between the lifted lip and pulled down lip from the t_0 to t_3 time interval about 80 FPS

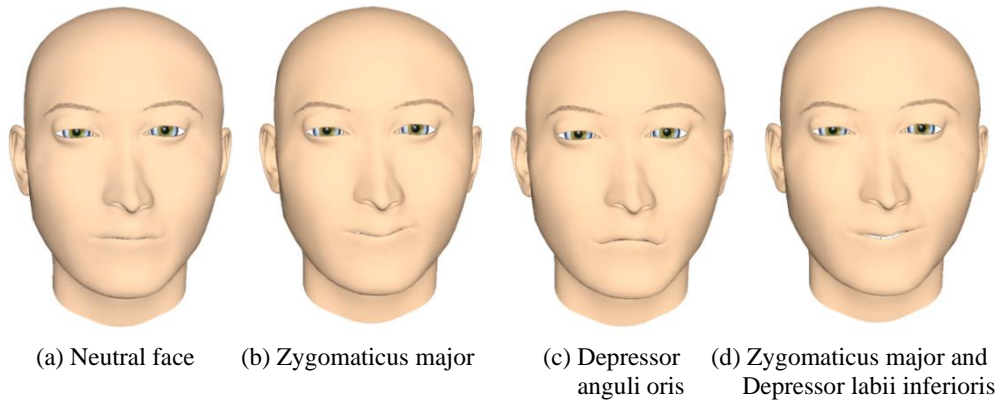


Figure 27. Facial animation with user-specific mesh

Table 4. FPS for various facial animations

	Gravity	Combined skin deformation		Transition
		Multiple muscles	Muscle and external force	
FPS	85	82	73	80

	Scalability		
	Zygomaticus major	Depressor anguli oris	Zygomaticus major and Depressor labii inferioris
FPS	82	85	73

VIII. Conclusion

We demonstrate real-time muscle-based facial animation using a novel facial framework based on modal warping for shell elements. With no need for extra equipment or handcrafted facial data, we implemented a physics-based facial simulation in real-time. Furthermore, as skin deformations are not only caused by muscle but also by soft tissue with high complexity, we keep anatomical characteristics of elastomers under the face in consideration.

To reconstruct the human face, we built a novel face model that is simplified to 4 layers including skin, muscle, subcutaneous fatty layer, and skull. We interpret skin and muscles as shell elements and designed a subcutaneous fatty layer using the mass-spring system. The forces exerted on skin generated by muscles are implemented as propagation through the tissue layer. Every facial component having dynamic models is integrated into the governing equation of skin deformation. In our system, according to the linear independence of the different types of external forces, the governing equation for combined skin deformation can be easily solved. Solving the governing equation by using the modal warping technique reduces DOFs of the equation for non-linear facial deformations so that simulations can be done in real-time.

As a result, muscles are explicitly built so that they are easy to import or export skin and muscles, and unwanted tessellation results are prevented by considering the thin structure of muscle. Mass-spring forces are generated in proportion to the amount of muscle deformations transferred to skin nodes through connected springs. With propagated force, the skin deforms according to the deformation direction of the muscle while the skin and muscles are fixed on the proper position of the skull. By decomposing the displacement field, various effects on the skin surface including gravity load, single expression by multiple muscles, and interactions with both external forces and muscle-driven forces can be shown as real-time animations.

As a limitation of our current work also as future work, we did not consider rigid body dynamics of the skull and jaw and their collision response; and jaw kinematics could be integrated. Also, solving inverse dynamics for controlling the muscle deformation could be another future work, yet we can control maximum muscle stretch with the experimental value. Integrating existing reconstruction techniques for more anatomically precise facial structure and applying non-linear constitutive model for the elastic body would be a challenging problem.

Bibliography

- [1] G. Barbarino, M. Jabareen, J. Trzewik, and E. Mazza, “Physically based finite element model of the face,” *Lect. Notes Comput. Sci. (including Subser. Lect. Notes Artif. Intell. Lect. Notes Bioinformatics)*, vol. 5104 LNCS, pp. 1–10, 2008.
- [2] B. Bickel *et al.*, “Multi-scale capture of facial geometry and motion,” in *ACM transactions on graphics (TOG)*, 2007, vol. 26, no. 3, p. 33.
- [3] T. Weise, H. Li, L. Van Gool, and M. Pauly, “Face/off: Live facial puppetry,” in *Proceedings of the 2009 ACM SIGGRAPH/Eurographics Symposium on Computer animation*, 2009, pp. 7–16.
- [4] J. P. Lewis, K. Anjyo, T. Rhee, M. Zhang, F. H. Pighin, and Z. Deng, “Practice and Theory of Blendshape Facial Models.,” *Eurographics (State Art Reports)*, vol. 1, no. 8, p. 2, 2014.
- [5] G. G. Barbarino, M. Jabareen, J. Trzewik, A. Nkengne, G. Stamatias, and E. Mazza, “Development and validation of a three-dimensional finite element model of the face,” *J. Biomech. Eng.*, vol. 131, no. 4, p. 41006, 2009.
- [6] T. Wu, A. Hung, and K. Mithraratne, “Generating facial expressions using an anatomically accurate biomechanical model,” *IEEE Trans. Vis. Comput. Graph.*, vol. 20, no. 11, pp. 1519–1529, 2014.
- [7] E. Sifakis, I. Neverov, and R. Fedkiw, “Automatic determination of facial muscle activations from sparse motion capture marker data,” in *Acm transactions on graphics (tog)*, 2005, vol. 24, no. 3, pp. 417–425.
- [8] A. E. Ichim, P. Kadleček, L. Kavan, and M. Pauly, “Phace: Physics-based face modeling and animation,” *ACM Trans. Graph.*, vol. 36, no. 4, 2017.
- [9] S. A. Maas, B. J. Ellis, G. A. Ateshian, and J. A. Weiss, “FEBio: finite elements for biomechanics,” *J. Biomech. Eng.*, vol. 134, no. 1, p. 11005, 2012.
- [10] Q. Zhu, Y. Chen, and A. Kaufman, “Real-time Biomechanically-based Muscle Volume Deformation using FEM,” *Comput. Graph. Forum*, vol. 17, no. 3, pp. 275–284, Aug. 1998.
- [11] J. Teran, S. Blemker, N. V. Thow Hing, and R. Fedkiw, “Finite volume methods for the simulation of skeletal muscle,” in *Proceedings of the 2003 ACM SIGGRAPH/Eurographics Symposium on Computer Animation, SCA 2003*, 2003.

- [12] J. Teran, E. Sifakis, G. Irving, and R. Fedkiw, “Robust quasistatic finite elements and flesh simulation,” in *Proceedings of the 2005 ACM SIGGRAPH/Eurographics symposium on Computer animation*, 2005, pp. 181–190.
- [13] B. Smith, F. De Goes, and T. Kim, “Stable neo-hookean flesh simulation,” *ACM Trans. Graph.*, vol. 37, no. 2, 2018.
- [14] J. Haber and D. Terzopoulos, “Facial modeling and animation,” in *ACM SIGGRAPH 2004 Course Notes*, 2004, p. 6.
- [15] K. Reed and D. Cosker, “User-Guided Facial Animation through an Evolutionary Interface,” in *Computer Graphics Forum*, 2019.
- [16] B. Bickel, M. Lang, M. Botsch, M. A. Otaduy, and M. Gross, “Pose-space animation and transfer of facial details,” in *Proceedings of the 2008 ACM SIGGRAPH/Eurographics Symposium on Computer Animation*, 2008, pp. 57–66.
- [17] T. Weise, S. Bouaziz, H. Li, and M. Pauly, “Realtime performance-based facial animation,” in *ACM transactions on graphics (TOG)*, 2011, vol. 30, no. 4, p. 77.
- [18] H. Li, J. Yu, Y. Ye, and C. Bregler, “Realtime facial animation with on-the-fly correctives,” *ACM Trans. Graph.*, vol. 32, no. 4, pp. 41–42, 2013.
- [19] T. Rhee, Y. Hwang, J. D. Kim, and C. Kim, “Real-time facial animation from live video tracking,” in *Proceedings of the 2011 ACM SIGGRAPH/Eurographics Symposium on Computer Animation*, 2011, pp. 215–224.
- [20] V. Orvalho, P. Bastos, F. I. Parke, B. Oliveira, and X. Alvarez, “A Facial Rigging Survey,” in *Eurographics (STARs)*, 2012, pp. 183–204.
- [21] A. Wojdeł and L. J. M. Rothkrantz, “Parametric generation of facial expressions based on FACS,” in *Computer graphics forum*, 2005, vol. 24, no. 4, pp. 743–757.
- [22] S. Villagrana and A. Sánchez, “Face! 3d facial animation system based on facs,” in *IV Iberoamerican symposium in computer graphics*, 2009, pp. 203–209.
- [23] D. Komorowski, V. Melapudi, D. Mortillaro, and G. S. Lee, “A hybrid approach to facial rigging,” in *ACM SIGGRAPH ASIA 2010 Sketches*, 2010, p. 42.
- [24] Y. Gao, Q. Zhao, A. Hao, T. M. Sezgin, and N. A. Dodgson, “Automatic construction of 3D animatable facial avatars,” *Comput. Animat. Virtual Worlds*, vol. 21, no. 3–4, pp. 343–354, 2010.
- [25] J. Bibliowicz, “An automated rigging system for facial animation,” Citeseer, 2005.
- [26] K. Waters, “A muscle model for animation three-dimensional facial expression,” *Acm*

- siggraph Comput. Graph.*, vol. 21, no. 4, pp. 17–24, 1987.
- [27] Y. Zhang and T. Sim, “Realistic and efficient wrinkle simulation using an anatomy-based face model with adaptive refinement,” in *International 2005 Computer Graphics*, 2005, pp. 3–10.
- [28] S. Pieper, J. Rosen, and D. Zeltzer, “Interactive graphics for plastic surgery: A task-level analysis and implementation,” in *Symposium on Interactive 3 D Graphics: Proceedings of the 1992 symposium on Interactive 3 D graphics*, 1992, vol. 1992, pp. 127–134.
- [29] I. A. Essa and A. P. Pentland, “Coding, analysis, interpretation, and recognition of facial expressions,” *IEEE Trans. Pattern Anal. Mach. Intell.*, vol. 19, no. 7, pp. 757–763, 1997.
- [30] D. Terzopoulos and K. Waters, “Physically-based facial modelling, analysis, and animation,” *J. Vis. Comput. Animat.*, vol. 1, no. 2, pp. 73–80, 1990.
- [31] Y. Lee, D. Terzopoulos, and K. Waters, “Realistic modeling for facial animation,” *Proc. ACM SIGGRAPH Conf. Comput. Graph.*, pp. 55–62, 1995.
- [32] E. Sifakis and J. Barbic, “FEM simulation of 3D deformable solids: a practitioner’s guide to theory, discretization and model reduction,” in *Acm siggraph 2012 courses*, 2012, p. 20.
- [33] E. Gladilin, S. Zachow, P. Deuflhard, and H.-C. Hege, “Anatomy-and physics-based facial animation for craniofacial surgery simulations,” *Med. Biol. Eng. Comput.*, vol. 42, no. 2, pp. 167–170, 2004.
- [34] V. Barrielle and N. Stoiber, “Realtime Performance-Driven Physical Simulation for Facial Animation,” in *Computer Graphics Forum*, 2019, vol. 38, no. 1, pp. 151–166.
- [35] M. G. Choi, S. Yong Woo, and H.-S. Ko, “Real-time simulation of thin shells,” in *Computer Graphics Forum*, 2007, vol. 26, no. 3, pp. 349–354.
- [36] M. G. Choi and H.-S. Ko, “Modal warping: Real-time simulation of large rotational deformation and manipulation,” *IEEE Trans. Vis. Comput. Graph.*, vol. 11, no. 1, pp. 91–101, 2005.
- [37] J. N. Reddy, “An introduction to the finite element method,” *New York*, 1993.
- [38] M. Bernadou, *Finite element methods for thin shell problems*. Wiley, 1996.
- [39] E. Grinspun, A. N. Hirani, M. Desbrun, and P. Schröder, “Discrete shells,” in *Proceedings of the 2003 ACM SIGGRAPH/Eurographics symposium on Computer animation*, 2003, pp. 62–67.
- [40] S. Standring, *Gray’s anatomy e-book: the anatomical basis of clinical practice*. Elsevier Health Sciences, 2015.

- [41] B. C. Mendelson and S. R. Jacobson, “Surgical anatomy of the midcheek: facial layers, spaces, and the midcheek segments,” *Clin. Plast. Surg.*, vol. 35, no. 3, pp. 395–404, 2008.
- [42] M. Chabanas, V. Luboz, and Y. Payan, “Patient specific finite element model of the face soft tissues for computer-assisted maxillofacial surgery,” *Med. Image Anal.*, vol. 7, no. 2, pp. 131–151, 2003.
- [43] J. W. Rohen, *Color atlas of anatomy: a photographic study of the human body*. Wolters Kluwen, 2011.
- [44] F. H. Netter, S. Colacino, and others, *Atlas of human anatomy*. Ciba-Geigy Corporation, 1989.
- [45] A. M. R. Agur and A. F. Dalley, *Grant’s atlas of anatomy*. Lippincott Williams & Wilkins, 2009.
- [46] M. Müller, J. Stam, D. James, and N. Thürey, “Real time physics: class notes,” in *ACM SIGGRAPH 2008 classes*, 2008, p. 88.

Appendix I

Edge extraction from .obj file

For edge-based energy function (equation (2) and equation (3)), extracting 4 indices information of edges from the .obj file is

Algorithm 1 Edge Extraction

```

1: procedure EDGEEXTRACTION
   Input: facets  $F$ , edges  $E$ 
   Output: edges  $E$ 
2:   for all  $i$  in  $F$  do
3:     for  $j = 1$  to  $3$  do
4:        $E_{tmp}.id[0] \leftarrow F[i].v[j]$ 
5:        $E_{tmp}.id[1] \leftarrow F[i].v[(j + 1)\%3]$ 
6:        $E_{tmp}.faceID.push(i)$ 
7:        $E.push(E_{tmp})$ 
8:     collect  $faceIDs$  to one edge for overlapping edges
9:     remove duplicated edges except storing  $faceIDs$ 
10:    for all  $i$  in  $E$  do
11:      if  $E[i].faceID.size() == 1$  then
12:         $E[i].id[2] \leftarrow$  the remain vertex of  $F[E[i].faceID[0]]$ 
13:         $E[i].id[3] \leftarrow -1$ 
14:      else
15:         $E[i].id[2] \leftarrow$  the remain vertex of  $F[E[i].faceID[0]]$ 
16:         $E[i].id[2] \leftarrow$  the remain vertex of  $F[E[i].faceID[1]]$ 

```

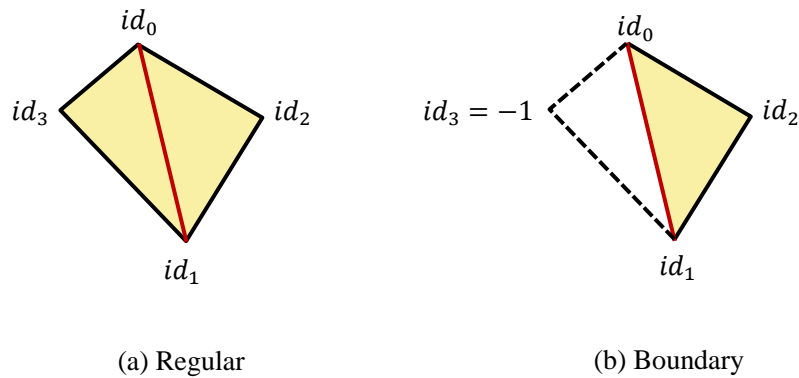


Figure 28. Edge indices information

Appendix II

Decomposition of the governing equation for the skin

By using equation (20), the governing equation (17) becomes

$$\begin{aligned} \mathbf{M}_{\mathbf{q}_s} \ddot{\mathbf{q}}_s + \mathbf{C}_{\mathbf{q}_s} \dot{\mathbf{q}}_s + \mathbf{K}_{\mathbf{q}_s} \mathbf{q}_s &= \Phi_s^T (\mathbf{R}_s^T \mathbf{F}_{ext_s}) \\ &= \Phi_s^T \left(\mathbf{R}_s^T \left\{ \mathbf{F}_{M_1} + \mathbf{F}_{M_2} + \cdots + \mathbf{F}_{M_k} + \mathbf{F}_{ext_{s_1}} + \mathbf{F}_{ext_{s_2}} + \cdots + \mathbf{F}_{ext_{s_l}} \right\} \right) \end{aligned} \quad (22)$$

$$\begin{aligned} &= \Phi_s^T (\mathbf{R}_s^T \mathbf{F}_{M_1}) + \cdots + \Phi_s^T (\mathbf{R}_s^T \mathbf{F}_{M_k}) + \\ &\Phi_s^T (\mathbf{R}_s^T \mathbf{F}_{ext_{s_1}}) + \cdots + \Phi_s^T (\mathbf{R}_s^T \mathbf{F}_{ext_{s_l}}). \end{aligned} \quad (23)$$

For $i \in \{1, \dots, k\}$ and $j \in \{1, \dots, l\}$, $k \in \mathbb{Z}^+$ and $l \in \mathbb{Z}^+$ are the index numbers of different muscles and different external forces except caused by muscle. According to the definition, equation (17) comes to

$$\begin{aligned} \mathbf{M}_{\mathbf{q}_s} \ddot{\mathbf{q}}_s + \mathbf{C}_{\mathbf{q}_s} \dot{\mathbf{q}}_s + \mathbf{K}_{\mathbf{q}_s} \mathbf{q}_s &= \Phi_s^T (\mathbf{R}_s^T \mathbf{F}_{ext_s}) \\ &= \left(\mathbf{M}_{\mathbf{q}_{M_1}} \ddot{\mathbf{q}}_{M_1} + \mathbf{C}_{\mathbf{q}_{M_1}} \dot{\mathbf{q}}_{M_1} + \mathbf{K}_{\mathbf{q}_{M_1}} \mathbf{q}_{M_1} \right) \\ &\quad + \cdots \\ &\quad + \left(\mathbf{M}_{\mathbf{q}_{M_k}} \ddot{\mathbf{q}}_{M_k} + \mathbf{C}_{\mathbf{q}_{M_k}} \dot{\mathbf{q}}_{M_k} + \mathbf{K}_{\mathbf{q}_{M_k}} \mathbf{q}_{M_k} \right) \\ &+ \left(\mathbf{M}_{\mathbf{q}_{ext_{s_1}}} \ddot{\mathbf{q}}_{ext_{s_1}} + \mathbf{C}_{\mathbf{q}_{ext_{s_1}}} \dot{\mathbf{q}}_{ext_{s_1}} + \mathbf{K}_{\mathbf{q}_{ext_{s_1}}} \mathbf{q}_{ext_{s_1}} \right) \\ &\quad + \cdots \\ &+ \left(\mathbf{M}_{\mathbf{q}_{ext_{s_l}}} \ddot{\mathbf{q}}_{ext_{s_l}} + \mathbf{C}_{\mathbf{q}_{ext_{s_l}}} \dot{\mathbf{q}}_{ext_{s_l}} + \mathbf{K}_{\mathbf{q}_{ext_{s_l}}} \mathbf{q}_{ext_{s_l}} \right). \end{aligned} \quad (24)$$

where \mathbf{q}_{M_i} and $\mathbf{q}_{ext_{s_j}}$ are the i -th and j -th modal amplitudes by \mathbf{F}_{M_i} and $\mathbf{F}_{ext_{s_j}}$.

As the governing equation produces displacement fields for external force types, we can say that

$$\begin{aligned} \mathbf{u}_s &= \mathbf{u}_{M_1} + \cdots + \mathbf{u}_{M_k} + \mathbf{u}_{ext_{s_1}} + \cdots + \mathbf{u}_{ext_{s_l}} \\ &= \sum_f \mathbf{u}_f. \end{aligned} \quad (25)$$

국문초록

김정민

컴퓨터공학과

이화여자대학교 대학원

얼굴 애니메이션은 가상 아바타, 영화 또는 게임 산업을 포함한 컴퓨터 애니메이션 분야에서 활용될 수 있으며 가상 안면 수술 시뮬레이터와 같이 의료 산업 응용 분야로의 확장성을 기대할 수 있다. 본 논문에서는 근육 변형을 이용한 실시간 물리 기반 얼굴 애니메이션을 제안한다. 3차원 유한 요소를 사용하는 이전 근육 기반 얼굴 애니메이션과 달리, 2차원 유한 요소인 쉘 요소를 사용하여 얇은 막 구조를 지닌 안면 근육을 해석하여 비효율적이고 부적절한 형태의 메쉬가 안면 근육을 구성하는 것을 방지한다. 또한 시뮬레이션의 실시간 성능을 위해 전통적으로 유한 요소 해석에서 다루는 복잡한 쉘 모델 대신 기하학적으로 파생된 쉘 모델과 에너지 함수를 도입하고 모드 위핑을 이용하여 미분 방정식으로 주어진 지배 방정식을 해석한다.

해부학적으로 유의미한 얼굴 애니메이션 결과를 위해, 제안하는 시스템은 인체 해부학 지식을 기반으로 피부, 피하 층, 근육 그리고 두개골로 구성된 4개 층을 얼굴 모델로 설계한다. 피부와 근육은 쉘 요소로 구성되며 쉘 요소 해석에 따른 역학 방정식의 지배를 받는다. 표피, 진피, 피하 지방 및 근막과 같은 복잡한 탄성체로 구성된 피부와 근육 사이의 피하 지방 조직은 질량-스프링 시스템을 이용하여 균일한 탄성체로 가정한다. 마지막으로 두개골과 연결된 근육 말단 부분은 정적 위치 제약 조건에 의해 고정된다.

안면 근육은 주로 수축과 이완의 변형을 이루기 때문에 본 시스템은 안면

근육의 지배 방정식에 대한 모드 해석 결과를 이용하여 근육이 인장력에 의한 변형만 이루도록 제어한다. 또한 근육의 변형으로 인해 파생된 힘이 피하 지방 조직을 움직이고 이를 통해 힘이 피부에 전달되어 피부가 변형을 이루게 된다. 제안된 시스템에서는 근육과 피부 노드를 연결하는 스프링의 질량-스프링 힘을 통해 피부 메쉬에 외력을 가함으로써 근육에 의한 피부 변형을 모방한다. 한편 근육이 갖는 피부와의 위치에 따라 근육으로부터 전달된 힘의 영향을 받는 피부 영역인 관심 영역을 정의함으로써, 적절한 부위의 피부가 해당 근육의 움직임에 따라 변형될 수 있도록 한다. 제안된 시스템에서 관심 영역 외의 피부 메쉬 노드는 정적 위치 제약 조건으로 통제되기 때문에, 다중 근육의 외력이 피부에 가해질 경우, 해당 근육의 관심 영역이 다른 근육에 의해 제약될 수 있다. 이를 방지하기 위해 피부에 가해지는 외력에 따라 지배 방정식을 독립적으로 분리하여 피부와 여러 근육이 상호작용할 수 있도록 시스템을 설계하였다.

본 연구는 역동적인 피부 변형과 연관 있는 근육을 선별하여 이로 인해 변형되는 일련의 안면 근육 기반 실시간 얼굴 애니메이션 결과를 제시한다. 또한 제안된 시스템은 새로운 근육이나 피부 메쉬의 삽입과 삭제가 용이하여 다양한 메쉬에 대해 확장성을 갖는다.

감사의 글

부족한 저에게 많은 가르침을 주신 김영준 교수님께 먼저 감사의 말씀드립니다. 종종 어디로 튈지 몰라 불안정했던 저에게 목표를 정하고 그 길을 찾아갈 수 있는 능력을 길러 주셨습니다. 또한 교수님께서 주신 다양한 학회와 세미나 기회를 통해 학문적 시야를 넓힐 수 있었고, 카멜레온 프로젝트를 통해서도 잊지 못할 기억을 얻었습니다. 연구를 진행함에 있어, 제가 흥미 있는 분야가 무엇인지를 가장 우선적으로 관심 가져 주시고, 또 믿고 맡겨 주심에 정말 감사드립니다. 아무것도 몰랐던 학부 인턴 시절부터, 마지막까지 저를 포기 않으시고 꼼꼼히 지도해 주시고 많은 것을 깨닫게 해주심에 감사드립니다. 그동안 교수님께서 보여주신 연구에 대한 열정과, 교수님께서 지도해주신 연구에 임하는 자세와 방향성 잊지 않고 나아가도록 하겠습니다.

그리고 최민규 교수님께 감사드립니다. 연구에 어려움이 있을 때 지도와 도움 주셔서 무사히 연구를 마칠 수 있었습니다. 갑작스럽게 찾아 뵈게 되었을 때에도 편히 대해 주시고, 난관에 봉착한 상황에서 모자란 부분을 채워 주심에 정말 감사드립니다. 변형체 연구에 가르침 주신 교수님의 식견에 감명을 받아 큰 깨달음을 얻을 수 있었습니다.

또한 논문 심사와 지도에 도움주신 박현석, 오유란 교수님께 감사드립니다. 바쁜 일정 중에 제 연구에 관심을 가져 주시고 많은 시간을 할애해 주셔서 감사합니다. 마지막까지 잘 마무리할 수 있도록 주신 지도와 격려의 말씀 큰 힘이 되었습니다. 3년 간 가족 보다 같이 한 시간이 많았던 연구실 식구들, 김예솔 언니, 민혜정 언니, 송다은, 김지수 언니, 김지선 언니, 김시연, 김민영 언니, 한경민 박사님, 유지연 선생님, 그리고 졸업하신 이영은 언니, 김여진 언니, 김윤형 언니, 김현정 언니, 김은희 선생님, 즐거웠던 순간들과 따뜻한 기억들을 선물해 주셔서 감사합니다. 제가 무너지지 않도록 옆에서 지켜 주셔서 감사합니다. 큰 숲과 같은 동료들

의 품이 있어 쉬어갈 수도, 나아갈 수도 있었습니다.

지난 1년이 넘는 시간 동안 저의 정신력과 체력을 책임지고 길러 주신 발레 서민영 선생님께도 감사의 말씀드립니다. 선생님의 즐겁고 열정적인 수업을 통해 긍정적이고 밝은 힘을 얻을 수 있었고, 정신없는 와중 저의 유일한 낙이자 스트레스를 해소할 수 있는 선물 같은 시간이었습니다. 잊지 않고 소중히 간직하겠습니다.

또한 방배동 친구들에게 감사드립니다. 기쁠 때나 슬플 때나 가장 먼저 달려와 주고, 먼 곳에서도 마음으로 함께 하며 큰 힘이 되어주어 항상 고마운 마음입니다. 뿐만 아니라 힘이 되어준 모든 친구들에게도 감사드립니다.

그리고 사랑하는 엄마, 외할머니, 아빠, 동생 민용이에게 감사드립니다. 묵묵히 곁을 지켜 주신 외가 친척분들께도 감사의 말씀드립니다. 가족이 있어 지난 모든 순간이 소중한 추억으로 간직되었고, 앞으로의 기쁨을 기대할 수 있었습니다.

마지막으로 저의 원동력이시고, 지금은 하늘에서 지켜보고 계실, 너무나 큰 사랑으로 저를 길러 주신 외할아버지께 사랑과 감사의 인사 올립니다.

김정민 올림